JBC RESEARCH ARTICLE

Xenophagy of invasive bacteria is differentially activated and modulated *via* a TLR-TRAF6-Beclin1 axis in echinoderms

Received for publication, October 15, 2021, and in revised form, January 13, 2022 Published, Papers in Press, February 2, 2022,
https://doi.org/10.1016/j.jbc.2022.101667

Yina Shao[1,‡], Zhenhui Wang[1,‡], Kaiyu Chen[1,‡], Dongdong Li[1], Zhimeng Lv[1], Chundan Zhang[1], Weiwei Zhang[1], and Chenghua Li[1,2,3,*]

From the [1]State Key Laboratory for Quality and Safety of Agro-products, Ningbo University, Ningbo, China; [2]Laboratory for Marine Fisheries Science and Food Production Processes, Qingdao National Laboratory for Marine Science and Technology, Qingdao, China; [3]State-Province Joint Laboratory of Marine Biotechnology and Engineering, Ningbo University, Ningbo, China

Edited by George DeMartino

In marine environments, organisms are confronted with numerous microbial challenges, although the differential regulation of xenophagy in response to different pathogenic bacterial species remains relatively unknown. Here, we addressed this issue using *Apostichopus japonicus* as a model. We identified 39 conserved autophagy-related genes by genome-wide screening, which provided a molecular basis for autophagy regulation in sea cucumbers. Furthermore, xenophagy of two Gram-negative bacteria, *Vibrio splendidus* and *Escherichia coli*, but not a Gram-positive bacteria, *Micrococcus luteus*, was observed in different autophagy assays. Surprisingly, a significantly higher autophagy capacity was found in the *E. coli*–challenged group than in the *V. splendidus*–challenged group. To confirm these findings, two different lipopolysaccharides, $LPS^{V.\ splendidus}$ and $LPS^{E.\ coli}$, were isolated; we found that these LPS species differentially activated coelomocyte xenophagy. To explore the molecular mechanism mediating differential levels of xenophagy, we used an siRNA knockdown assay and confirmed that $LPS^{V.\ splendidus}$-mediated xenophagy was dependent on an *Aj*TLR3-mediated pathway, whereas $LPS^{E.\ coli}$-mediated xenophagy was dependent on *Aj*Toll. Moreover, the activation of different *Aj*TLRs resulted in *Aj*TRAF6 ubiquitination and subsequent activation of K63-linked ubiquitination of *Aj*Beclin1. Inversely, the $LPS^{V.\ splendidus}$-induced *Aj*TLR3 pathway simultaneously activated the expression of *Aj*A20, which reduced the extent of K63-linked ubiquitination of *Aj*Beclin1 and impaired the induction of autophagy; however, this finding was no t evident with $LPS^{E.\ coli}$. Our present results provide the first evidence showing that xenophagy could be differentially induced by different bacterial species to yield differential autophagy levels in echinoderms.

Autophagy is a highly conserved and mostly selective intracellular degradation pathway in eukaryotes that is mainly involved the regulation of essential physiological processes (1–3). For autophagy activation, a portion of the cytoplasmic component is first surrounded by a cup-shaped structure called the phagophore (4, 5), and this phagophore then extends, closes, and forms a double-membrane autophagosome (6). Subsequently, autophagosomes fuse with lysosomes (in metazoan cells) or vacuoles (in yeast and plant cells) to degrade cytoplasm-derived materials by lysosomal/vacuolar hydrolases. Various autophagy-related genes and multiple signaling pathways are involved in these processes (7). Among these core sets of proteins, LC3/Atg8 are widely adopted as molecular markers to determine the occurrence of autophagy (8). Recent studies have shown that autophagy can selectively degrade specific cargoes *via* processes referred to as "selective autophagy," which aim to maintain cellular homeostasis, regulate inflammatory responses, and eliminate invasive pathogens (9, 10). Special terms have been coined to describe selective autophagy according to the types of targeted cargoes, and these terms include mitophagy (mitochondria), pexophagy (peroxisomes), lipophagy (lipid droplets), aggrephagy (protein aggregates), and xenophagy (invading microorganisms) (10).

Xenophagy, a unique type of selective autophagy, has received extensive attention and plays a central role in innate immunity by targeting foreign entities, such as viruses, bacteria, and parasites and protecting host cells from fatal damage (11). In mammals, different types of pathogenic bacteria, including *Salmonella enterica* (12), *Listeria monocytogenes* (13), *Shigella flexneri* (14), and *Helicobacter flexneri* (15), distinctly lose the "battle" in different models and reportedly induce xenophagy. Interestingly, nearly all invading microbe-induced xenophagy is dependent on an interaction between the bacterial cell wall components and pattern recognition receptors (PRRs) in host cells, which provides the missing link between pathogen recognition and the initiation of autophagy (16–18). For instance, Khan *et al.* (19) demonstrated that two types of scavenger receptors, macrophage receptor with collagenous structure (MARCO) and scavenger receptor-B1 (SR-B1), in human mesenchymal stem cells (MSCs) could mediate xenophagy and enhance the intracellular killing of the pathogen by binding to lipoglycans from *Mycobacterium tuberculosis*. Travassos *et al.* (20) found that nucleotide-binding oligomerization domain 1 (NOD1) and NOD2 of the family of NOD-like receptors (NLRs) in human epithelial HeLa cells activate xenophagy after specifically binding to peptidoglycan (PGN) from *S. flexneri* and *L. monocytogenes*. Toll/Toll-

‡ These authors contribute equally to this work.
* For correspondence: Chenghua Li, lichenghua@nbu.edu.cn.

© 2022 THE AUTHORS. Published by Elsevier Inc on behalf of American Society for Biochemistry and Molecular Biology. This is an open access article under the CC BY-NC-ND license (http://creativecommons.org/licenses/by-nc-nd/4.0/).

like receptors (TLRs) are considered the most important PRRs in mediating xenophagy. Delgado *et al.* (18) screened a pathogen-associated molecular pattern (PAMP) ligand library for effects on xenophagy in murine macrophage cell lines and found that different TLRs could identify different ligands from bacteria or viruses (*i.e.*, TLR3 can identify polyinosinic-polycytidylic acid [poly(I:C)], TLR2 can identify zymosan, and TLR4 can identify LPS) to active xenophagy. However, lipopeptides such as Pam_3CSK_4 (TLR1/2 ligands), flagellin (TLR5 ligand), or CpG oligonucleotides (TLR9 ligand) cannot induce xenophagy. Moreover, TLR ligands induce xenophagy in a mainly cell-type-dependent manner, and the degradation mechanism of the cargoes might also differ among various species. For instance, single-stranded RNA (ssRNA) serves as a ligand for murine TLR7 and human TLR8 but is not recognized by human TLR7 (21) or murine TLR8 (22) in macrophages; thus, ssRNA cannot induce autophagy. In contrast, the same ligands from different bacteria might bind to different receptors to mediate xenophagy. In *Drosophila* primary hemocytes and S2 cells, two types of PGNs derived from different types of cells, DAP-type (from *Lactobacillus plantarum*) and lysine-type (from *Staphylococcus epidermidis*), can induce autophagy, but the receptor of peptidoglycan-recognition protein-LE (PGRP-LE) was responsible only for the induction of autophagy stimulated by DAP-type PGN, which suggests that cytoplasmic sensors other than PGRP-LE detect invading bacteria with cell walls containing lysine-type PGN (23, 24). Although the fundamental mechanism linking one pathogen with the autophagy machinery has been well studied, the mechanism through which host cells use distinct sensors to induce xenophagy in response to two or more microbes is largely unknown.

After the specific binding between PAMPs from microbes and PRRs from the host, the ubiquitination of some key autophagy-related proteins and cargoes is an important step for the formation of autophagosomes and subsequent autophagic degradation *via* xenophagy (7). TRAF6, as an E3 ubiquitin ligase, is widely involved in autophagy induction due to its autoubiquitination and heteroubiquitination activities (25). The stimulation of TLR4 and TLR3 with LPS and poly(I:C), respectively, triggers autophagy in lung cancer cells, which enhances the production of various cytokines by promoting TRAF6 ubiquitination and thus facilitates immune defense against pathogens (26). Moreover, accumulating evidence indicates that Beclin1 is the principal substrate of the ubiquitin ligases that regulate the autophagy machinery (27). K63-ubiquitination of Beclin1 promotes autophagy induction (28) but K48-linked ubiquitin to induce a negative pathway for autophagy regulation (29). Upon TLR engagement, TRAF6 promotes the K63-linked ubiquitination of Beclin1, Beclin1 is a core component of the class III phosphatidylinositol 3-kinase complex (PI3KC3), and the K63-linked ubiquitination of Beclin1 modulates the lipid kinase activity of PI3KC3 and thereby induces autophagy (25, 30). More importantly, the engagement of TLRs also triggers a signaling pathway that leads to the translocation of NF-κB to the nucleus and promotes the expression of A20. A20 contains an N-terminal ovarian tumor (OTU) deubiquitinase domain that removes K63-polyubiquitin chains from TRAF6 to turn off the activation of autophagy (25, 31, 32), which indicates that A20 negatively regulates TLR-induced autophagy in human cells.

Aquatic organisms are confronted with numerous microbial challenges in their living environments, including pathogenic, nonpathogenic, and beneficial challenges. Despite the importance of xenophagy in innate immunity, which directly captures pathogens or indirectly mediates immune responses to control foreign microbe infection (16, 33), the mechanism regulating xenophagy in response to different bacterial infections in the same species is largely unknown. To address this knowledge gap between xenophagy and host innate immune responses in aquatic organisms, we used *Apostichopus japonicus*, an economically important marine species, as a model. The sea cucumber *A. japonicus* is a marine invertebrate belonging to the Echinodermata and widely distributed in China, Korea, and other Asian countries. These species play important roles in ecology and aquaculture, they provide commodity or medicine valued by humans, including food resources (34). In China, the gross production of *A. japonicus* reached as high as 196,564 tons in 2020 and obtained remarkable economic. Moreover, they occupy a taxonomic position that is believed to be important for understanding the origin and evolution of deuterostomes. Considering the important role of xenophagy in resisting microorganisms, we decided to investigate the different bacteria in the regulation of sea cucumber autophagy. In this study, we confirmed that two Gram-negative bacteria, *Vibrio splendidus* and *Escherichia coli*, showed differential capacity to regulate xenophagy *via* different TLR cascades, whereas the Gram-positive bacterium *Micrococcus luteus* could not activate autophagy activity. The molecular basis for the different autophagy levels induced by the two Gram-negative bacteria was also elucidated. The findings obtained in this study will provide valuable insights into the autophagy mechanisms through which xenophagy and innate immunity pathways intersect and their contribution to cell survival in marine invertebrate species.

Results

Sea cucumbers have a complete autophagy machinery

The occurrence of autophagy in vertebrates involves four main successive steps, namely autophagy initiation, phagophore elongation, autophagosome formation, and lysosome fusion, and many key proteins and adaptors are involved in these processes (35). In our previous study, we found that the mRNA expression of several autophagy-related genes, such as *AjULK*, *AjAtg13*, *AjBeclin1*, and *AjLC3*, was significantly changed after *V. splendidus* challenge, which indicates that sea cucumbers might regulate autophagy-related genes and activate autophagy to resist pathogen invasion (36). However, whether the complete machinery needed for the autophagy process exists in *A. japonicus* is largely unknown. To understand whether sea cucumber has the molecular basis for the autophagy machinery, key proteins encoding genes involved in autophagy regulation were screened from sea cucumber

ASBMB

transcriptome (37) and genomes (38, 39), and the sequences were used for *in silico* analysis and sequence alignment. In our study, we ultimately identified 39 Atgs in *A. japonicus* that belong to the five complexes implicated in the four major steps, namely initiation, elongation, completion, and fusion of the autophagosome (Table S1). The results in Figure 1 show the key proteins involved in the core molecular mechanism of autophagy in *A. japonicus*, and their amino acid sequences were conserved compared with those of *Homo sapiens*, *Mus musculus*, *Danio rerio*, and *Strongylocentrotus purpuratus*. Among these autophagy-related proteins, LC3 plays an important role in the elongation of the autophagosome because its cleavage and its lipidation protein product (LC3-II) decorate autophagosomes. Animal LC3 proteins comprise two subfamilies: microtubule-associated protein 1 light chain 3 (LC3A/B/C), gamma-aminobutyric acid receptor–associated protein (GABARAP)/Golgi-associated ATPase enhancer of 16 kDa (GATE16) (8). Our sequence data for sea cucumber included four homologous genes, *Aj*LC3, *Aj*LC3C, *Aj*GABARAP, and *Aj*GABARAPL2 (Table S1), and we found that all four proteins contain an ATG8 domain and a highly conserved glycine residue in C-terminal, which suggests that the sea cucumber LC3 conjugation system might have a function similar to that of other conserved LC3 proteins in eukaryotes (Fig. 1 and Table S1). The sequence alignment revealed that *Aj*LC3 exhibited 70% identity with *H. sapiens* LC3B, and *Aj*LC3C exhibited 56.7% identity with *H. sapiens* LC3C. In addition, autophagy receptors initiate isolation membrane formation by bridging ubiquitinated substrates and LC3 *via* their ubiquitin-binding region (UBR) and ATG8/LC3-interacting region (LIR), respectively. In our case, the two primary receptors *Aj*p62/SQSTM1 and *Aj*NBR1 contained a UBR domain with an LIR motif at the C terminus (Fig. 1). In general, these results indicated that sea cucumbers possess the complete autophagy machinery and could be able to respond to bacterial infection.

Autophagy is activated by challenge with two Gram-negative bacteria of V. splendidus and E. coli but not a Gram-positive bacteria of M. luteus

Selective autophagy is a homeostatic regulation system that can specifically recognize substrates and play an antibacterial role in the immune response of the host (40). However, the xenophagy mechanism in response to other specific microbes found in aquatic environments is relatively unknown. Therefore, sea cucumber coelomocyte was challenged with three types of bacteria, *V. splendidus*, *E. coli*, and *M. luteus*, and the autophagy levels were detected by transmission electron microscopy (TEM). At 24 h after introduction of three bacteria into sea cucumbers, we observed double-membraned autophagosomes enclosed *V. splendidus* and *E. coli* within coelomocyte under Bafilomycin A1 (Baf-A1) treatment, but not in *M. luteus*–challenged group (Fig. 2*A*). The percentage of

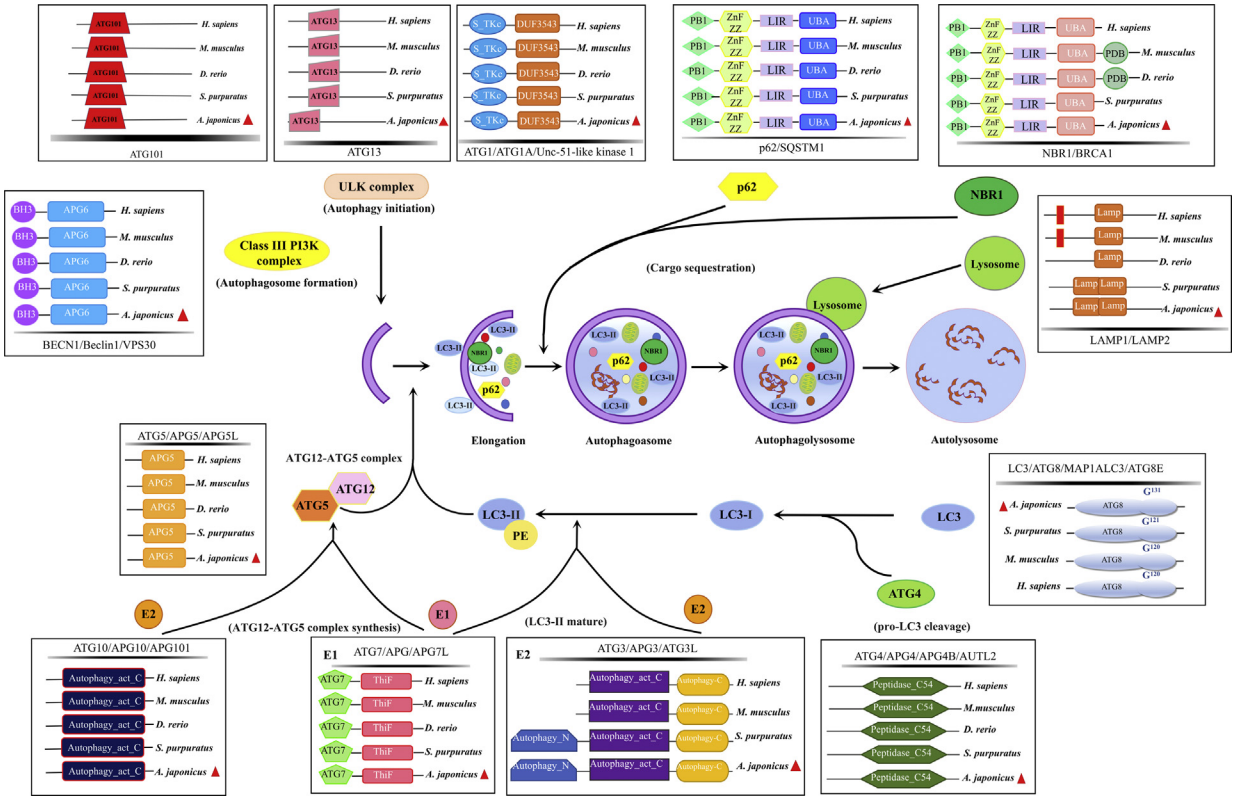

Figure 1. Complete autophagy machinery of *A. japonicus* according to *in silico* analysis. Sea cucumbers contain the main processes of autophagy, namely autophagy initiation, phagophore elongation, autophagosome formation, and lysosome fusion, and the presence of all processes guarantees the integrity of the autophagy machinery and the accomplishment of xenophagy. The domains of 13 key proteins were detected using the SMART program and compared with those of *Homo sapiens*, *Mus musculus*, *Danio rerio*, and *Strongylocentrotus purpuratus*.

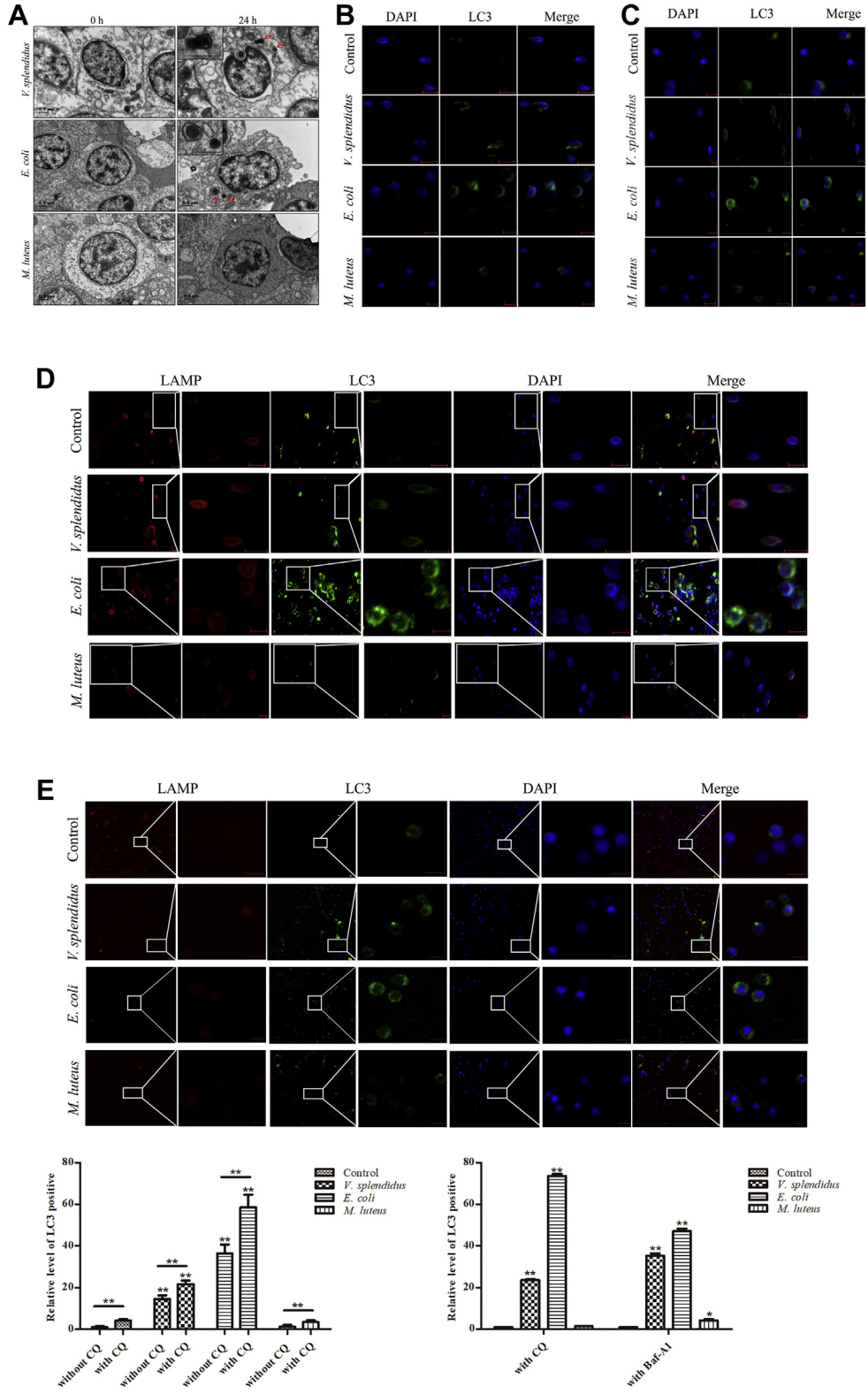

Figure 2. Characterization of *A. japonicus* coelomocyte xenophagy after challenge with *V. splendidus*, *E. coli*, and *M. luteus* for 24 h. *A*, TEM detection after *V. splendidus* and *E. coli* injection following with 10 nM Baf-A1 treatment, the *red arrows* indicated the double-membraned autophagosomes surrounding bacteria; *B*, LC3 fluorescence intensity detection without CQ or Baf-A1 injection; *C*, LC3 fluorescence intensity detection with CQ injection; *D*, LC3-positive autophagosomes colocalized with lysosomes with CQ injection. *E*, LC3-positive autophagosomes colocalized with lysosomes with Baf-A1 injection. After challenge, the cells were fixed and stained with anti-LC3 or combined with anti-LAMP antibodies at the indicated time point of 24 h. After nuclear staining with DAPI, *green* and *red signals* that represent autophagosomes and lysosomes, respectively, were visualized under a confocal microscope and statistically analyzed; scale bar = 5 μm. The relative LC3 positivity in 1000 cells from each indicated sample was determined. The data are presented as the means ± SDs ($n = 3$) relative to the control (0 h), are shown in bar graphs (*lower panel* in *D* and *E*). *Asterisks* indicate significant differences compared with the control group: $^{*}p < 0.05$ and $^{**}p < 0.01$ (*t* test).

intracellular bacteria in autophagosomes reached 7.8 ± 1.8% in *V. splendidus* group and 10.2 ± 2.7% in *E. coli* group when compared with control (0 h) group. Furthermore, Western blotting analysis indicated that the *Aj*LC3-II/I level was significantly increased at 12 (1.41-fold and 1.65-fold, $p < 0.01$) and 24 h (1.67-fold, $p < 0.01$ and 2.22-fold, $p < 0.01$) after challenge with *V. splendidus* and *E. coli* compared with the level in the 0 h (control) (Fig. 3, *B* and *C*), but *M. luteus* did not trigger an elevation in the lipidation of *Aj*LC3 (Fig. 3*A*). An autophagy receptor protein of *Ajp*62 exhibited significant decreases at 24 h post *E. coli* (0.69-fold, $p < 0.01$) and *V. splendidus* (0.76-fold, $p < 0.05$) challenge compared with the level in the 0 h (Fig. 3, *B* and *C*), but this change was not detected in *M. luteus*–challenged sea cucumber coelomocyte (Fig. 3*A*). Moreover, we found that the *Aj*LC3-II/I ratio in three bacteria challenged groups was significantly increases for Baf-A1 treatments, and the *Ajp*62 proteins were also measured and showed increased levels for Baf-A1 (Fig. 3). Besides, an immunofluorescence analysis indicated a significant increase in LC3 green fluorescence at 24 h after *V. splendidus* and *E. coli* challenge, but no significantly vivid spots were observed in *M. luteus*–challenged coelomocyte (Fig. 2*B*). The LC3-positive signal was significantly increased by 14.6- ($p < 0.01$) and 36.5-fold ($p < 0.01$) in the *V. splendidus* and *E. coli* groups, respectively. What is more, we found that the fluorescence intensity was clearly increased by Chloroquine (CQ) (Fig. 2*C*) in bacteria-infected sea cucumber coelomocyte and in the control group compared with that obtained without the injection of CQ (Fig. 2*B*), which suggested that bacteria induce functional degradative autophagy in *A. japonicus*. Moreover, to further verify the occurrence of autophagic flux in coelomocyte of *A. japonicus*, the accumulate LC3-positive puncta (*Aj*LC3) induced by CQ or Baf-A1 was detected by immunofluorescence observation. Double-staining analysis indicated that the red fluorescence representing lysosomal membranes and the green signal representing autophagosomal membranes were colocalized at 24 h post *V. splendidus* and *E. coli* challenge (Fig. 2, *D* and *E*). The quantitative results showed that

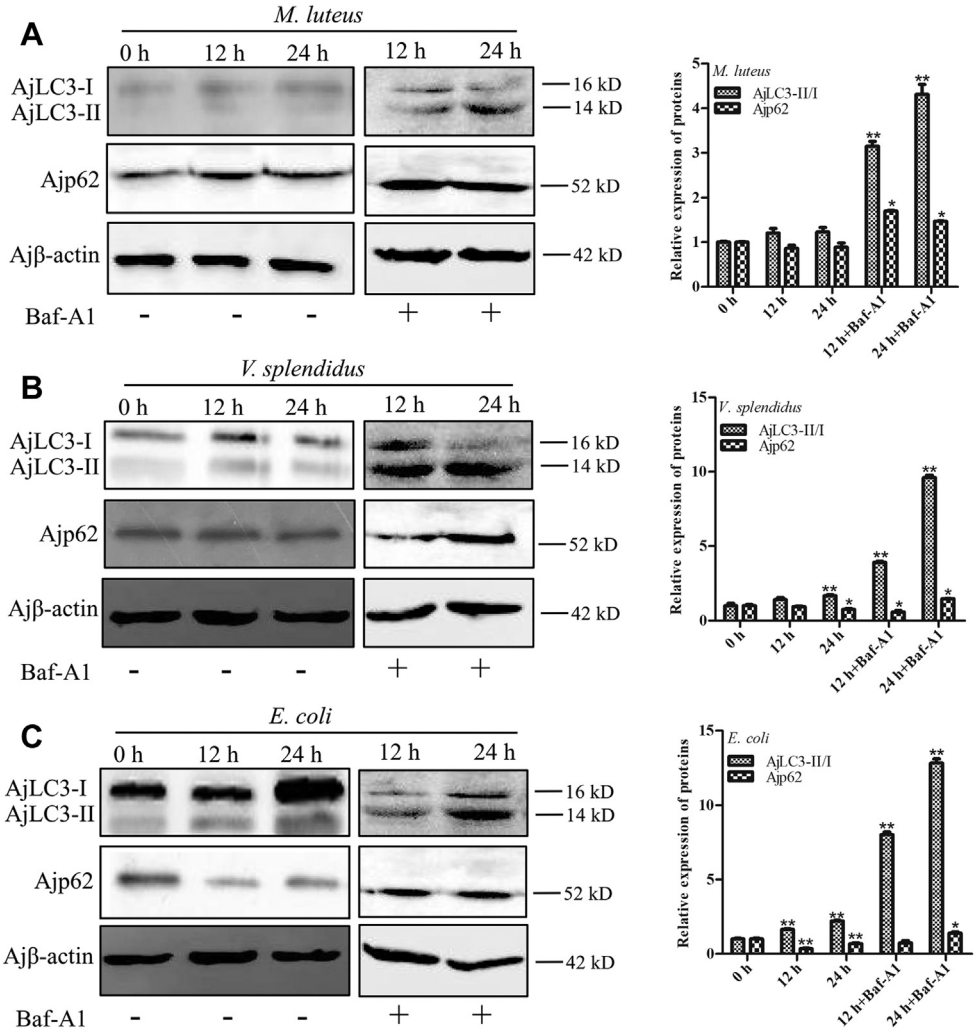

Figure 3. Characterization of *A. japonicus* coelomocyte xenophagy after challenge with *M. luteus*, *V. splendidus*, and *E. coli* by Western blotting analysis. Sea cucumbers were injected with or without 10 nM Baf-A1 following *M. luteus* (*A*), *V. splendidus* (*B*), and *E. coli* (*C*) challenge for 12 and 24 h, respectively. The protein band density was calculated using ImageJ software. The data, which are presented as the means ± SDs ($n = 3$) relative to the 0 h (control), are shown in bar graphs (*right panel* in *D* and *E*). *Asterisks* indicate significant differences compared with the control group: *$p < 0.05$ and **$p < 0.01$ (*t* test).

the LC3-positive signal was markedly upregulated by 23.6-fold ($p < 0.01$) and 73.5-fold ($p < 0.01$) in the *V. splendidus* and *E. coli* groups based on CQ treatments (Fig. 2*D*). And the LC3 green fluorescence was significantly increased by 35.2-fold ($p < 0.01$) in the *V. splendidus* group and 47.0-fold ($p < 0.01$) in the *E. coli* group under Baf-A1 treatments compared with that in the control group (Fig. 2*E*). All these results supported the conclusion that two Gram-negative bacteria, *V. splendidus* and *E. coli*, but not *M. luteus*, could induce xenophagy. Interestingly, the autophagy levels induced by *E. coli* were significantly higher than those induced by *V. splendidus* according to the number of autophagosomes, LC3 punctum formation, LC3-II/I ratio, and protein levels of two autophagy receptors (Figs. 2 and 3).

LPS from V. splendidus *and* E. coli *differentially induce xenophagy*

LPS has been widely considered an important selective autophagy induction factor that regulates specific downstream cargoes and is targeted to the degradation pathway (41). To address the differential autophagy levels induced by *V. splendidus* and *E. coli* depending on their different LPS sources, we isolated the LPSs from *V. splendidus* and *E. coli*. Equal final concentrations of LPS (10 μg ml^{-1}) were added to cultured coelomocyte followed by Baf-A1 treatments, and we found that both LPSs could promote autophagosome formation (Fig. 4*A*). Furthermore, the *Aj*LC3-II/I level was significantly increased at 6 and 12 h after $LPS^{E.\ coli}$ exposure, and the protein level of *Aj*p62 was markedly decreased under the same condition, respectively (Fig. 4*B*). Similarity, the *Aj*LC3-II/I level was also markedly increased after $LPS^{V.\ splendidus}$ stimulation, following with decreased expression of *Aj*p62 (Fig. 4*B*). What is more, significant increases in *Aj*LC3-II/I and *Aj*p62 were both observed after Baf-A1 exposures, with the higher magnitudes in $LPS^{E.\ coli}$ group (Fig. 4*B*). To confirm whether autophagic flux occurred after LPS stimulation, the accumulated LC3 green signal was also measured by immunofluorescence following CQ or Baf-A1 treatment. Our results showed that the fluorescence intensity of *Aj*LC3 was significantly increased at 12 h after the exposure of the coelomocyte to $LPS^{E.\ coli}$ following CQ (23.5-fold, $p < 0.01$) (Fig. 4*C*) and Baf-A1 (29.7-fold, $p < 0.01$) treatments (Fig. 4*D*). Moreover, the LC3 fluorescence intensity in $LPS^{V.\ splendidus}$ stimulation group was also observably increased by 3.66-fold ($p < 0.01$) with CQ (Fig. 4*C*) and 6.82-fold ($p < 0.01$) with Baf-A1 at 12 h (Fig. 4*D*) compared with those in the control group. Besides, we found that the LC3 green signal in the $PGN^{M.\ luteus}$ group showed a slight increase after Baf-A1 treatment (Fig. 4*D*). To prove that the observed LC3 green signal is indeed autophagosome, we silenced *AjULK* by siRNA and analyzed the changes in autophagy marker expression and LC3 green fluorescence. To be mentioned, the *AjULK* was successfully silenced in our previous work, and the autophagy flux in coelomocyte was markedly decreased after *AjULK* knockdown *in vivo* (36). Here, the *Aj*LC3-II/I level (Fig. 5) and LC3 immunofluorescence (Fig. 6*H*) were both damaged after interference of *AjULK* based on two different LPS stimulations, whereas the *Aj*p62 level was significantly increased under the same condition (Fig. 5), suggesting that the observed LC3 puncta are really autophagosomes but not LC3-associated phagocytosis. Based on the overall results, we concluded that the different LPSs from *V. splendidus* and *E. coli* both induced coelomocyte xenophagy in *A. japonicus* and that $LPS^{E.\ coli}$ stimulation and *E. coli* challenge induced a higher autophagic flux (Figs. 2–4).

Differential LPS-induced autophagy is dependent on different TLR cascades

To understand whether differential LPS-induced autophagy was activated by different PRR-mediated signaling pathways, we silenced the four identified PRRs, *AjTLR3*, *AjToll*, *AjNLRC4*, and *AjSR-B*, and analyzed the changes in autophagy marker expression (*Aj*LC3 lipidation and *Aj*p62 degradation) based on the two different LPS stimulations (Figs. 5 and S1). All of these PRRs were found to bind to LPS in previous work (42–44). Our results indicated that $LPS^{V.\ splendidus}$ exposure did not change the *Aj*LC3-II/I and *Aj*p62 levels in the *AjTLR3*-knockdown group (Fig. 5*A*). In contrast, we found that the *Aj*LC3-II/I and *Aj*p62 levels were significantly increased and decreased, respectively, in a time-dependent manner in the *AjToll*-, *AjNLRC4*-, and *AjSR-B*-silenced groups and in the control (0 h) group (Fig. 5*A*), which supported the finding that $LPS^{V.\ splendidus}$ induced autophagy through *Aj*TLR3 signaling. With $LPS^{E.\ coli}$, no changes in *Aj*LC3 lipidation and *Aj*p62 degradation were detected in the *AjToll*-silenced group but not in the *AjTLR3*-, *AjNLRC4*-, and *AjSR-B*-silenced groups or the control (0 h) group (Fig. 5*B*). Overall, the results indicated that $LPS^{V.\ splendidus}$ and $LPS^{E.\ coli}$ induced xenophagy *via* the *Aj*TLR3-and *Aj*Toll-mediated signal cascades, respectively.

TLRs mediate LPS-induced xenophagy via *the TRAF6-Beclin1 axis*

TRAF6, as an important adaptor in the TLR signaling pathway, plays broad roles during immune responses, such as inflammatory cytokine secretion and autophagy initiation (45, 46). In our study, the protein expression of *Aj*TRAF6 was significantly increased after 12 h of exposure to $LPS^{V.\ splendidus}$ and $LPS^{E.\ coli}$ (Figs. 6, *A* and *B* and S2, *A* and *B*). Furthermore, we found that the K63-linked ubiquitination level of *Aj*TRAF6 in the $LPS^{V.\ splendidus}$ group was markedly increased at 12 h (Figs. 6*A* and S2*A*), and greater upregulation of this level was found in $LPS^{E.\ coli}$ group (Figs. 6*B* and S2*B*). In order to determine whether ubiquitination of *Aj*TRAF6 induced by TLR signaling pathways, the protein and K63-linked ubiquitination levels of *Aj*TRAF6 were analyzed after *AjTLR3* or *AjToll* knockdown following with two types of LPS challenges. We found that the *Aj*TRAF6 protein expression and K63-linked ubiquitination level were both damaged in *AjTLR3* (Figs. 6*C* and S2*C*) and *AjToll* knockdown groups (Figs. 6*D* and S2*D*) following two different LPS challenges; moreover, the expression of *Aj*TRAF6 and its ubiquitination level were also abolished after the silencing of *AjTRAF6* under

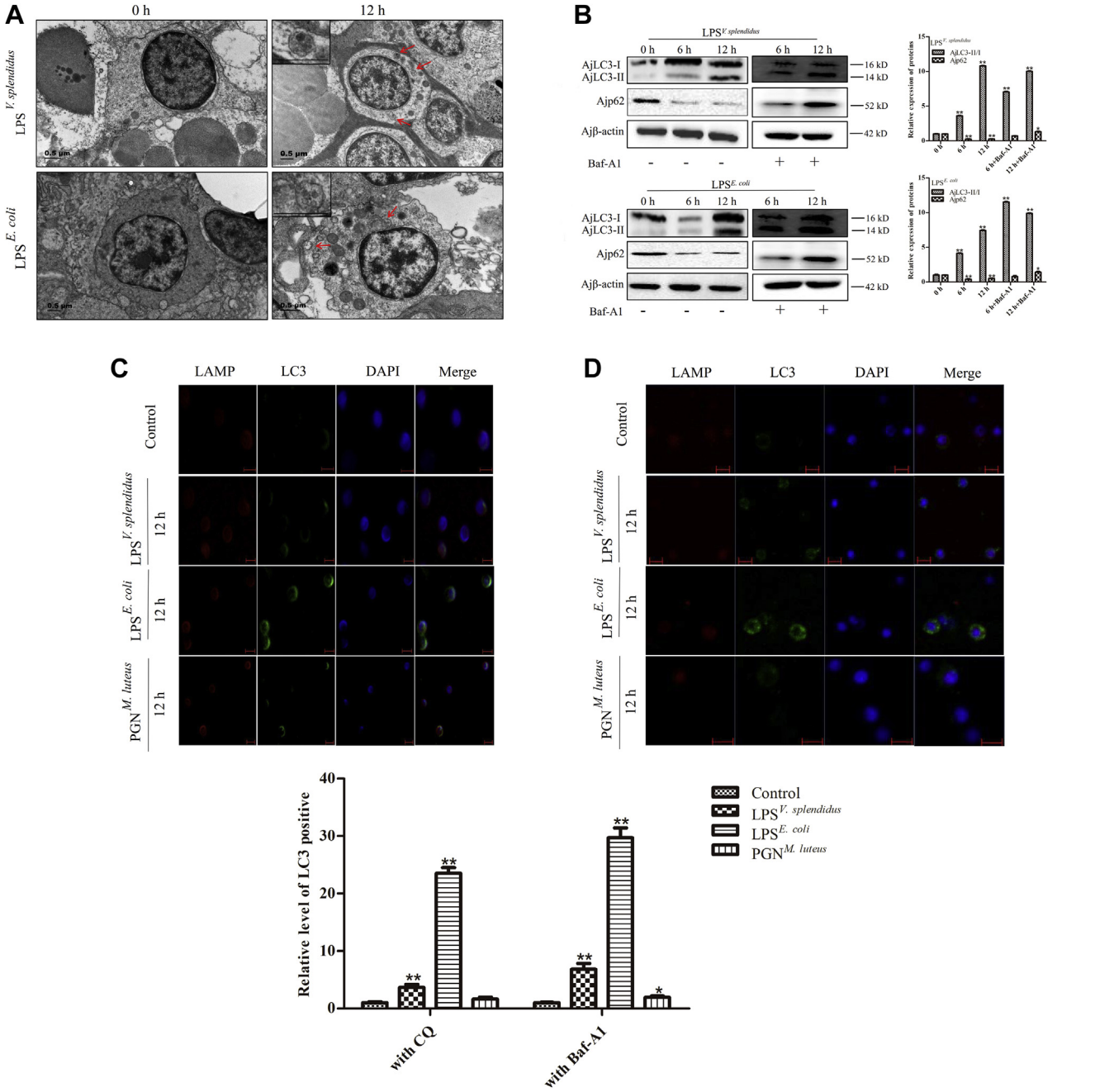

Figure 4. Characterization of *A. japonicus* primary coelomocyte xenophagy after LPS$^{V.\ splendidus}$, LPS$^{E.\ coli}$ and PGN$^{M.\ luteus}$ exposure. Primary cultured coelomocyte were exposed to LPS$^{V.\ splendidus}$, LPS$^{E.\ coli}$, and PGN$^{M.\ luteus}$ at a final concentration of 10 μg ml^{-1}, and the coelomocytes were collected at 0 h (control), 6, and 12 h following with CQ or Baf-A1 treatments for subsequent autophagy assays. *A*, TEM detection after LPS$^{V.\ splendidus}$ and LPS$^{E.\ coli}$ exposure following with 2 nM Baf-A1 treatment, the *red arrows* indicated autophagosomes; *B*, Western blotting analysis after LPS$^{E.\ coli}$ and LPS$^{V.\ splendidus}$ exposure following with 2 nM Baf-A1 treatment; *C*, autophagosome (LC3) and lysosome (LAMP) colocalization detection with CQ treatment. *D*, autophagosome (LC3) and lysosome (LAMP) colocalization detection with Baf-A1 treatment. The protein band density was calculated using ImageJ software. The data, which are presented as the means ± SDs (n = 3) relative to the 0 h, are shown in bar graphs (*right panel* in *B*). For LC3-positive autophagosomes colocalized with lysosomes, the cells were fixed and stained with anti-LC3 in combination with anti-LAMP antibodies at the indicated time points (0 and 12 h). After nuclear staining with DAPI, green and red signals that represent autophagosomes and lysosomes, respectively, were visualized under a confocal microscope and statistically analyzed; scale bar = 5 μm. The relative LC3 positivity in 1000 cells from each indicated sample was determined. The data are presented as the means ± SDs (n = 3) relative to the control, are shown in bar graphs (*lower panel* in *C* and *D*). *Asterisks* indicate significant differences compared with the control group: *$p < 0.05$ and **$p < 0.01$ (t test).

LPS$^{V.\ splendidus}$ (Figs. 6*E* and S2*E*) and LPS$^{E.\ coli}$ challenges (Figs. 6*F* and S2*F*), as well as decreased expression of *Aj*LC3-II/I (Figs. 6, *E* and *F* and S2, *E* and *F*) and impaired LC3 green signal (Fig. 6*G*) under the same conditions. Our results suggested that *Aj*TRAF6 serves as a common adaptor for the two TLR signaling pathways (Figs. 6 and S2).

More importantly, Beclin1 is a critical component of the autophagy initiation machinery that is ubiquitinated by TRAF6

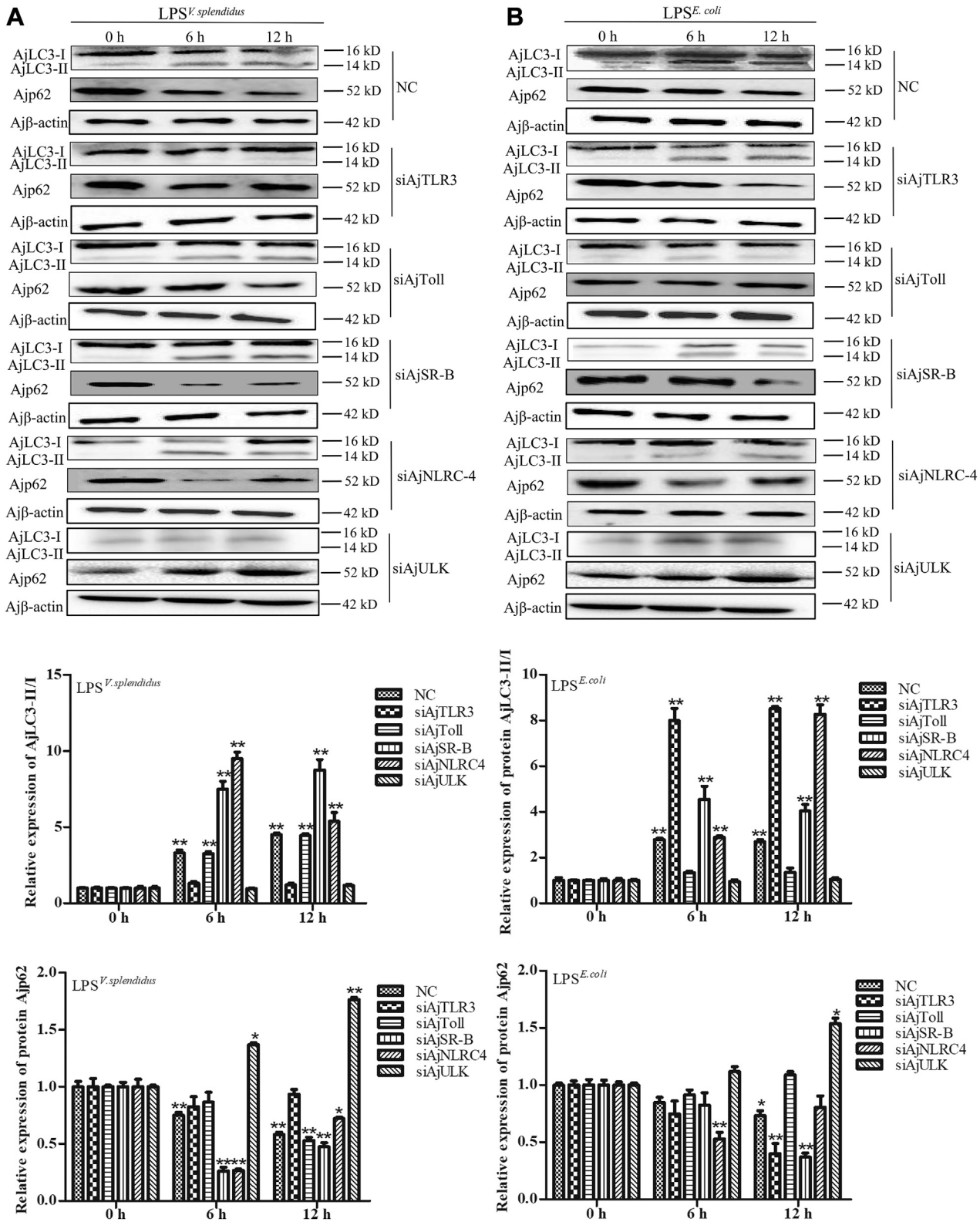

Figure 5. The *Aj*LC3-I-to-*Aj*LC3-II conversion and protein level of *Ajp62* in coelomocyte were detected after 0, 6, and 12 h of exposure to LPS$^{V.\ splendidus}$ and LPS$^{E.\ coli}$ following the mRNA silencing of *AjTLR3, AjToll, AjSR-B, AjNLRC-4,* and *AjULK*. *A*, Western blotting analysis of LPS$^{V.\ splendidus}$-challenged group following mRNA silencing of *AjTLR3*, *AjToll*, *AjSR-B*, *AjNLRC-4*, and *AjULK*; *B*, Western blotting analysis of LPS$^{E.\ coli}$-challenged group following mRNA silencing of *AjTLR3*, *AjToll*, *AjSR-B*, *AjNLRC-4*, and *AjULK*. The NC group was transfected with nontargeted double-stranded siRNA and served as the control. The protein band density was calculated using ImageJ software. The data, which are presented as the means ± SDs ($n = 3$) relative to the 0 h (control) are shown in bar graphs (*lower panel* in *A* and *B*). The *asterisks* indicate significant differences compared with the control group: *$p < 0.05$ and **$p < 0.01$ (*t* test).

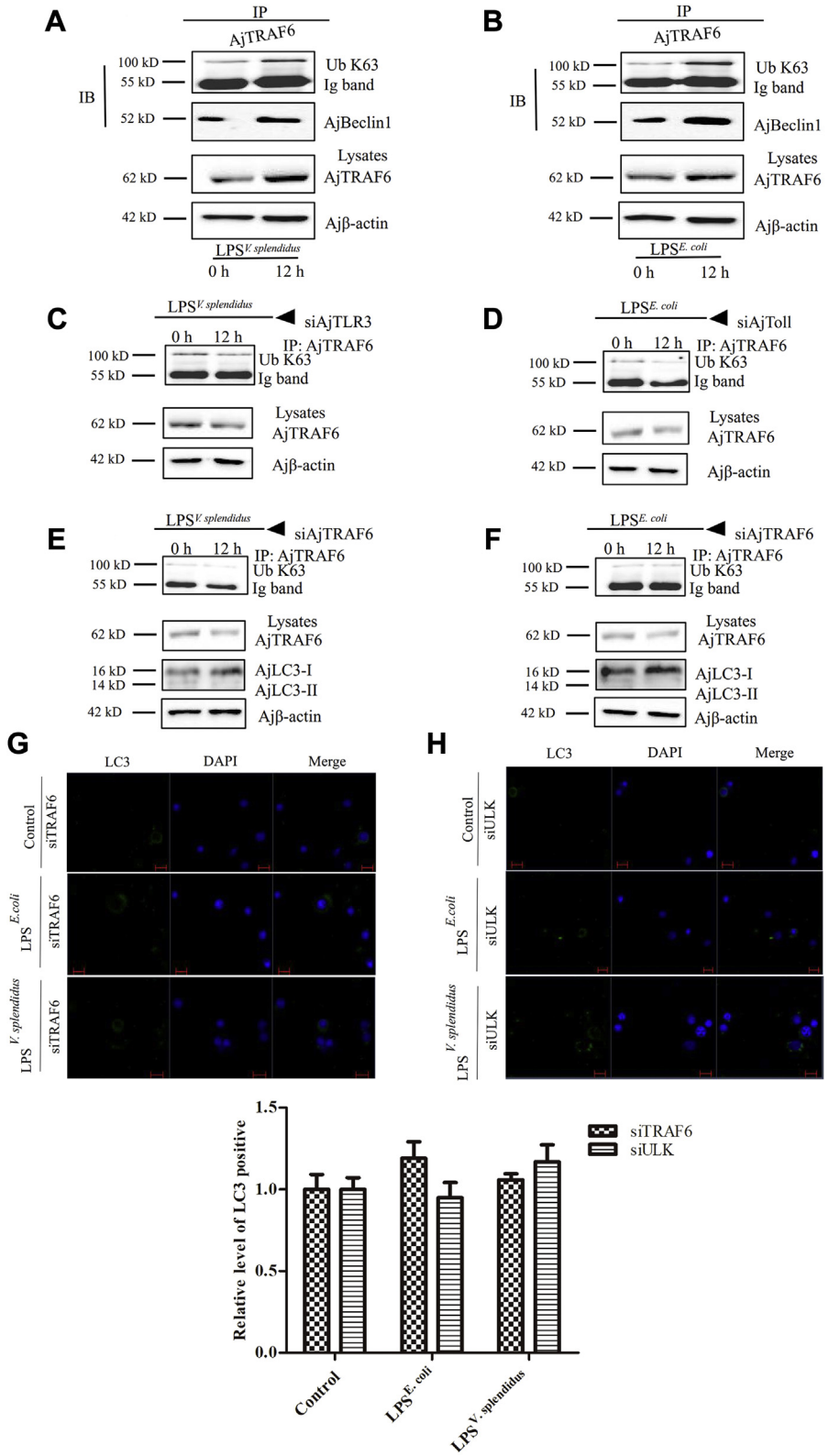

Figure 6. LPS$^{V.\ splendidus}$ and LPS$^{E.\ coli}$ mediate the K63-linked ubiquitination of *Aj*TRAF6 based on *Aj*TLR3 and *Aj*Toll cascades, which interacts with *Aj*Beclin1 to regulate xenophagy in *A. japonicus* coelomocyte. Sea cucumber primary coelomocyte were stimulated with LPS$^{V.\ splendidus}$ (*A*) or LPS$^{E.\ coli}$ (*B*) for the indicated times (0 and 12 h) following *AjTLR3* (*C*), *AjToll* (*D*), and *AjTRAF6* (*E* and *F*) silencing for 24 h. *G*, LC3 fluorescence intensity detection after interference of *AjTRAF6* followed by LPS$^{V.\ splendidus}$ or LPS$^{E.\ coli}$ exposure for 12 h. *H*, LC3 fluorescence intensity detection after interference of *AjULK* followed by LPS$^{V.\ splendidus}$ or LPS$^{E.\ coli}$ exposure for 12 h. Western blotting analysis of immunoprecipitated (IP) *Aj*TRAF6 samples was performed to determine the presence of K63-linked ubiquitin (Ub K63). The membranes in (*A*) and (*B*) were stripped and analyzed for interaction with *Aj*Beclin-1. Whole-cell lysates were analyzed by western blotting as indicated. The protein band density was calculated using ImageJ software. The heavy chain of the TRAF6 antibody was detected by the secondary antibody and was labeled Ig band. The data, which are presented as the means ± SDs (n = 3) relative to the 0 h (control) in Fig. S2. For LC3 positive signal, the cells were fixed and stained with anti-LC3 at the indicated time points (0 and 12 h). After nuclear staining with DAPI,

(25, 47). Thus, we explored *Aj*TRAF6-mediated xenophagy depending on *Aj*Beclin1 ubiquitination in sea cucumber coelomocyte. First, we found that the K63-linked ubiquitination of *Aj*Beclin1 was also markedly increased under the same conditions (Figs. 7, *A* and *B* and S3, *A* and *B*). Then, we determined the K63-linked ubiquitination of *Aj*Beclin1 after *AjTLR3* or *AjToll* silencing and found that *AjTLR3* or *AjToll* knockdown by specific siRNA impaired the LPS-induced K63-linked ubiquitination of *Aj*Beclin1 (Figs. 7, *C* and *D* and S3, *C* and *D*), which suggested that *Aj*TLR3 and *Aj*Toll mediate $LPS^{V.\ splendidus}$- and $LPS^{E.\ coli}$-induced ubiquitination of *Aj*Beclin1 in sea cucumber coelomocyte. To further determine whether the ubiquitination of *Aj*Beclin1 was dependent on its interaction with *Aj*TRAF6 in coelomocyte, we analyzed the interaction between *Aj*TRAF6 and *Aj*Beclin1 through an immunoprecipitation assay. The protein level of *Aj*Beclin1 after $LPS^{V.\ splendidus}$ or $LPS^{E.\ coli}$ stimulation was detected by Western blotting after precipitation with an *Aj*TRAF6-specific antibody (Figs. 6, *A* and *B* and S2, *A* and *B*). Notably, the expression of *Aj*Beclin1 and its ubiquitination level were both abolished after *AjTRAF6* silencing in the $LPS^{V.\ splendidus}$ group (Figs. 7*E* and S3*E*) as well as in $LPS^{E.\ coli}$ challenge group (Figs. 7*F* and S3*F*). Our findings indicated that *Aj*TRAF6 could directly ubiquitinate *Aj*Beclin1, which results in its ubiquitination, and promote autophagy during challenge with different types of LPSs.

AjTLR3 but not AjToll promotes the expression of the autophagy inhibitor AjA20

We have demonstrated that *Aj*TLR3 and *Aj*Toll are consistently involved in the regulation of autophagy by the *Aj*TRAF6-*Aj*Beclin1 axis during exposure to $LPS^{V.\ splendidus}$ and $LPS^{E.\ coli}$, whereas the mechanism underlying the differential autophagy capacity in response to these two Gram-negative bacteria remains unknown. A20, as a deubiquitination enzyme, has been proven to hinder the K63-linked ubiquitination of Beclin1 and further inhibit autophagy (25). In this study, the protein expression level of *Aj*A20 was significantly increased in coelomocyte after 12 h of exposure to $LPS^{V.\ splendidus}$ (Figs. 7*A* and S3*A*), and its level was also significantly increased in the *AjTRAF6*-silenced group upon $LPS^{V.\ splendidus}$ challenge (Figs. 7*E* and S3*E*); these observations indicated that *Aj*A20 might play a negative role in the regulation of autophagy induction. Moreover, we found that the elevation in the protein level of *Aj*A20 was abolished by the knockdown of *AjTLR3* under the same conditions (Figs. 7*C* and S3*C*), which suggested that *Aj*TLR3 signaling promotes *Aj*A20 expression under $LPS^{V.\ splendidus}$ stimulation. However, the analysis of *E. coli*–mediated autophagy showed that the exposure of coelomocyte to $LPS^{E.\ coli}$ did not trigger changes in *Aj*A20 expression (Figs. 7*B* and S3*B*), and no changes were obtained with *AjToll* (Figs. 7*D* and S3*D*) or *AjTRAF6* (Figs. 7*F* and S3*F*) silencing under the same conditions.

Discussion

Xenophagy is a particularly important type of selective autophagy and plays a pivotal role in host innate immune defense. Unlike bulk degradation of the packaged cargo in nonselective autophagy, xenophagy imparts selectivity to the degradation process by tagging and targeting cargoes into lysosomes (17). In mammalian species, the role of xenophagy in selectively eliminating disease-related pathogens, such as mycobacteria (19), HIV (48), and toxoplasma (49), has been well studied. However, the differential regulation mechanisms of xenophagy in response to different microbe challenges in a specific species, particularly an aquatic animal, remain largely unknown. In this study, 39 conserved Atgs were obtained by screening the sea cucumber genome, and the results indicated that *A. japonicus* possesses the complete machinery necessary for the autophagy process. We further found that the two Gram-negative bacteria *V. splendidus* and *E. coli* induced differential TLR-dependent xenophagy *via* their different LPSs, but the Gram-positive bacteria *M. luteus* did not induce xenophagy. Both autophagy pathways were dependent on activation of the TLR-TRAF6-Beclin1 axis through the ubiquitination of *Aj*Beclin1. Moreover, *V. splendidus*–induced autophagy also increased the expression of the deubiquitinase *Aj*A20, which impaired the K63-linked ubiquitination of *Aj*Beclin1, but this cascade was not detected in the $LPS^{E.\ coli}$-induced *Aj*Toll signaling pathway. Overall, our current study provides novel insights into the xenophagic mechanism through which different TLR-TRAF6-Beclin1 axis initiates autophagy in marine invertebrates.

Because *A. japonicus* lacks an adaptive immune system, this species must employ its innate immune system to protect itself against infections. The release of the genome of *A. japonicus* (38, 39) allowed us to identify autophagy-related proteins of sea cucumbers. Therefore, using multiple sequence alignment and SMART tools, we observed that the core proteins involved in the autophagy pathway appear to be functional in *A. japonicus* and could be divided into four main steps: initiation, phagophore elongation, autophagosome formation, and lysosome fusion (Fig. 1 and Table S1). Among all Atg-encoded proteins, LC3/Atg8 is one of the most important ubiquitin-like proteins that is synthesized as a precursor with a key Gly residue at its C terminus (called LC3-I), which is cleaved by Atg4 and ultimately forms mature LC3-II *via* reactions mediated by Atg3 and Atg7 (8). In our study, we found four LC3 homologs from *A. japonicus* (named *Aj*LC3, *Aj*LC3C, *Aj*GABARAP, and *Aj*GABARAPL2), and all of these shared a highly conserved ATG8 domain with other species, such as *S. purpuratus* and *H. sapiens*. Although these four LC3 homologs also shared a conserved Gly site in their C terminus with other LC3 proteins, the position of this key site in *A. japonicus* (*Aj*LC3 in Gly^{131}, *Aj*LC3C in Gly^{117}, *Aj*GABARAP in Gly^{116}, and *Aj*GABARAP in Gly^{129}) is slightly different from that in the referenced species (consistently Gly^{120}). This

green signal represents autophagosomes was visualized under a confocal microscope and statistically analyzed; scale bar = 5 μm. The relative LC3 positivity in 1000 cells from each indicated sample was determined. The data are presented as the means ± SDs ($n = 3$) relative to the control, are shown in bar graphs (*lower panel* in *G* and *H*). The *asterisks* indicate significant differences compared with the control group: $^{*}p < 0.05$ and $^{**}p < 0.01$ (*t* test).

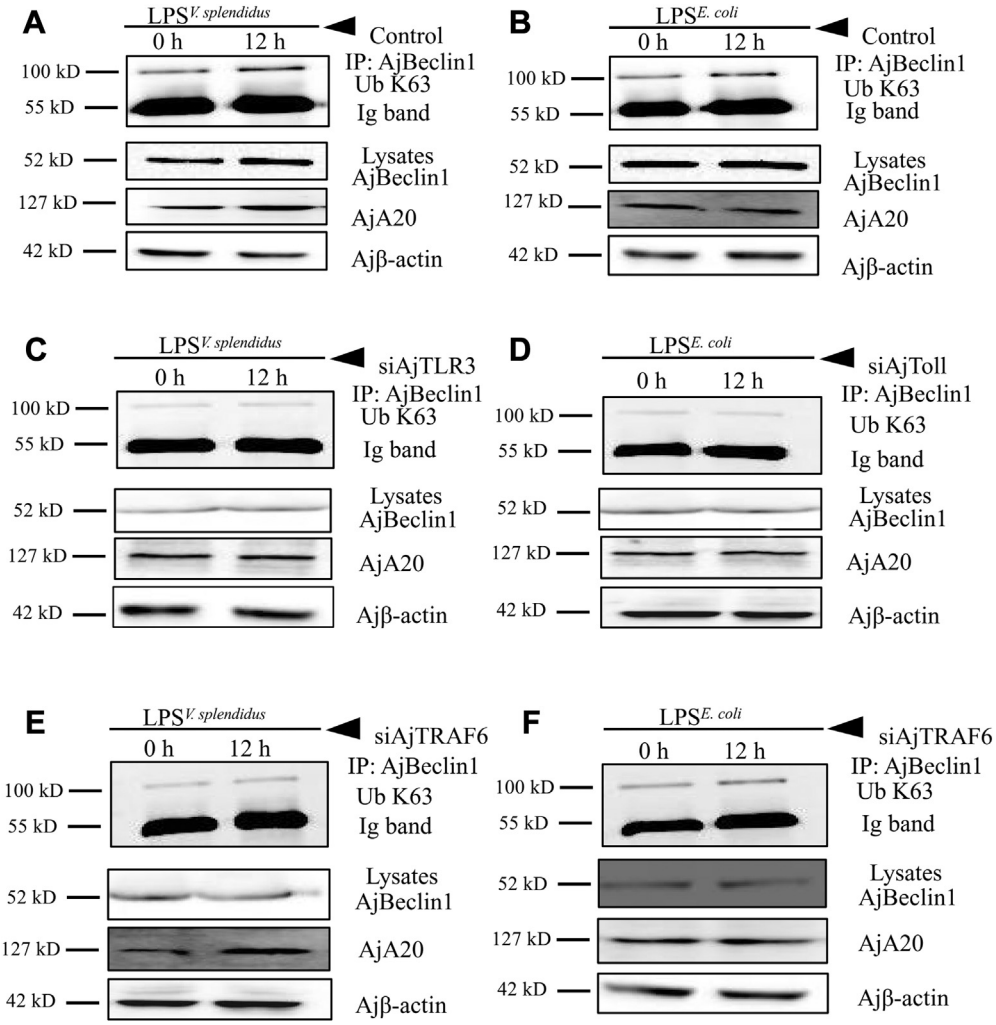

Figure 7. LPS$^{V.\ splendidus}$ and LPS$^{E.\ coli}$ differentially induce *A. japonicus* coelomocyte xenophagy by *Aj*A20. Sea cucumber primary coelomocyte were stimulated with LPS$^{V.\ splendidus}$ (*A*) or LPS$^{E.\ coli}$ (*B*) for the indicated times (0 and 12 h) following *AjTLR3* (*C*), *AjToll* (*D*), and *AjTRAF6* (*E* and *F*) silencing for 24 h. Western blotting analysis of immunoprecipitated (IP) *Aj*Beclin1 samples was performed to determine the presence of K63-linked ubiquitin (Ub K63). Whole-cell lysates were analyzed by western blotting as indicated. The protein band density was calculated using ImageJ software. The heavy chain of the Beclin1 antibody was detected by the secondary antibody and was labeled Ig band. The data are presented as the means ± SDs ($n = 3$) relative to the 0 h (control) in Fig. S3. The V indicate significant differences compared with the control group: *$p < 0.05$ and **$p < 0.01$ (*t* test).

difference in the position of the residue appears to not affect its cleavage by Atg4 but might decide its functional differentiation in other types of autophagy (50). Moreover, Beclin1 is the mammalian homologue of yeast Atg6, a key component of PI3KC3 that initiates autophagy by helping localize other autophagy proteins to the preautophagosomal membrane (51). The K63-linked ubiquitination of Beclin1 at Lys^{117} facilitates the oligomerization of Beclin-1 and enhances the lipid kinase activity of PI3KC3 (25, 51). In our study, *Aj*Beclin1 showed good conservation with Beclin1 from other species and contained an Lys residue at position 115, a key target for linking ubiquitin chains. Furthermore, the xenophagy-mediated elimination of cytoplasmic cargoes depends on recognition by specialized receptors known as xenophagy adaptors (52). Almost all adaptors in mammals contain one or more ubiquitin-binding domains (UBDs, including UBA) and an LIR (53). In *A. japonicus*, the two xenophagy adaptors *Aj*p62 and *Aj*NBR1 include a UBD and an LIR motif, which is consistent with the results found for mammalian species proteins. To date, several structures of LC3 orthologs bound to LIR motifs, including a crystal structure of LC3B bound to the p62 or NBR1 LIR peptide, have been analyzed, and the noncanonical LIR (CLIR) motif in the autophagy receptor NDP52 binds to LC3C (53). In our study, we could not find the NDP52 gene in the sea cucumber genome. Moreover, we concluded that the *Aj*LC3 sequence was closer to that of LC3B, which binds to p62 or NBR1 to induce autophagy through the LIR motif. Therefore, we prepared human LC3B antibody to analyze sea cucumber coelomocyte autophagy during bacterial infection. We observed the accumulation of *Aj*LC3-II/I and the formation of double-layer autophagosomes, and these findings were further confirmed by the degradation of *Aj*p62 after *V. splendidus* challenge. These data strongly indicate the existence of autophagic flux in *A. japonicus* (Figs. 2 and 3), which indicates that sea cucumbers possess a complete autophagy machinery similar to other advanced species.

Xenophagy is differentially modulated by TLR-TRAF6-Beclin1

Although the existence of complete autophagy machinery provides a molecular basis for the occurrence of xenophagy in *A. japonicus*, whether autophagy could be activated by different types of microbes remains largely unknown. Therefore, we investigated the autophagic flux in *A. japonicus* exposed to three different bacteria. Our results clearly indicated that two types of Gram-negative bacteria could induce coelomocyte xenophagy, but the Gram-positive bacteria *M. luteus* failed to activate xenophagy in *A. japonicus* (Figs. 2 and 3). Gibson *et al.* (54) showed that the Gram-positive bacteria *Staphylococcus aureus* could induce xenophagy in zebrafish. Moreover, Yano *et al.* (23) showed that *Drosophila* lacking PGRP-LE or expressing mutant PGRP-LE^{112} was unable to undergo autophagy, which resulted in increased susceptibility to *L. monocytogenes* infection. Recently, we found only a short-type PGRP (named *Aj*PGRP-S) in the sea cucumber genome (55), and further analysis indicated that the key site of *Aj*PGRP-S is not conserved to counterpart in *Drosophila*. Therefore, we speculated that this failure of *M. luteus*–induced xenophagy could be explained by the fact that the bacterial ligand might not be recognized by *Aj*PGRP-S.

Nearly all inductions of autophagy by invading microbes are dependent on the interaction between bacterial cell wall components and PRRs of host cells (16–18). In our study, we found that the two Gram-negative bacteria differentially induced xenophagy, and a higher autophagy ratio was found in the *E. coli* group. In addition, the *Aj*LC3-II/I ratio, the p62 protein level, and LC3 green signal were all significantly increased by CQ and Baf-A1 injections. As well known, Baf-A1 and CQ are commonly used that inhibit autophagy flux by targeting the lysosomes, which indicated that bacterial infection induced degradative xenophagy in *A. japonicus*. To date, most studies have primarily focused on the xenophagic mechanism of the host in response to infection with a single pathogen (19, 56). Juárez *et al.* (57) showed that NOD2 enhances the autophagy of alveolar macrophages after *M. tuberculosis* infection in humans. Moreover, Liu *et al.* (58) indicated that *Salmonella typhimurium*–induced autophagy in a RAW264.7 murine macrophage cell line is mediated by the TLR4 signaling pathway. In TLR4-deficient macrophages, LPS (from *S. Typhimurium*) is unable to induce autophagy. More importantly, the abovementioned studies demonstrated that LPS, flagellin, and CpG oligodeoxynucleotides from Gram-negative bacteria other than *Salmonella* activate TLR4, TLR5, and TLR9, respectively, and induce different degrees of autophagy in RAW264.7 cells. In our study, we suspected that the significant differences in the induction of autophagy might depend on different PRR signaling pathways that are activated by PAMPs from different bacteria to increase the expression of autophagy-related molecules (25, 26). LPS is a complex glycolipid endotoxin derived from the cell wall of Gram-negative bacteria (59) and is a powerful inducer of autophagy in many mammalian cell lines, including macrophages (60), hepatocytes (41), and myoblasts (61). First, to confirm that the mediation of autophagy by the two Gram-negative bacteria was dependent on LPS, we performed an autophagy assay using cultured coelomocyte and found that LPS$^{E.\ coli}$ and LPS$^{V.\ splendidus}$ induced autophagy in cultured sea cucumber coelomocyte (Fig. 4), which is consistent with the effects of the two bacteria on xenophagy. Multiple studies have shown that LPS induces autophagy through TLR cascades (58, 62). Wang *et al.* (63) demonstrated that the activation of autophagy by LPS *via* TLR4 represents an innate defense mechanism for controlling intracellular *E. coli* replication in human peritoneal mesothelial cells. However, only two TLRs, namely *Aj*TLR3 and *Aj*Toll, have been identified in sea cucumbers (42). Subsequently, to determine whether differential LPS-induced accumulation of autophagosomes occurs *via* PRRs in *A. japonicus*, we detected the autophagy levels after silencing four types of PRRs, including *AjNLRC4* and *AjSR-B*. Our results clearly indicated that *Aj*LC3 lipidation and *Aj*p62 degradation were highly correlated with the level of *Aj*TLR3 after LPS$^{V.\ splendidus}$ exposure and the level of *Aj*Toll after LPS$^{E.\ coli}$ stimulation (Fig. 5), respectively, which indicated that LPS$^{V.\ splendidus}$ induced coelomocyte xenophagy through *Aj*TLR3 and that LPS$^{E.\ coli}$ interacts mainly with *Aj*Toll to accelerate autophagy. Norris *et al.* (64) used different types of LPS (from several strains of *Burkholderia pseudomallei*) to challenge RAW264.7 cells and found that green LC3 signal was visible in all the groups but was markedly more abundant in 576a-, MSHR435-, and *Salmonella* LPS-treated cells. However, the differential autophagy levels in RAW264.7 cells mediated by different TLR cascades are largely unknown. In general, LPSs containing different components might induce differential activation of TLR2 and TLR4 to facilitate the elimination of invading bacteria through autophagy (65). LPS consists of three parts: lipid A, a core oligosaccharide, and an O side chain (66). Among these parts, the shape of the lipid A component determines the bioactivity of LPS (67). In our study, the differential autophagy levels induced by different bacteria indicated that the constituents of lipid A in these two types of LPSs might differ. Netea *et al.* (68) demonstrated that an LPS with a conical shape (*e.g.*, the LPS of *E. coli*) induces cytokine production through TLR4; however, a cylindrical LPS (*e.g.*, that of *Porphyromonas gingivalis*) induces cytokine expression through TLR2. In addition, Nahori *et al.* (69) showed that parental leptospiral LPS (*e.g.*, the LPS of *Leptospira interrogans*) was the predominant ligand for TLR1/TLR2 in human cells, whereas TLR2 and TLR4 contribute to activation in murine cells. Our results showed that the LPS from *E. coli* was mainly linked to *Aj*Toll in sea cucumbers, and a previous study demonstrated that *Aj*Toll exhibits high conservation with human TLR4 (46), which indicates that *Aj*Toll was similar to human TLR4 and likely induced by the conical LPS from *E. coli*. Usually, double-stranded RNA (dsRNA) or its synthetic analog poly(I:C) acts as a ligand of TLR3 and stimulates autophagy in various mammalian cells (18, 26, 60). Our analysis of the sequence characteristics of *Aj*TLR3 revealed that the pivotal amino acid residues for phosphorylation, which are necessary for the dsRNA-mediated signaling pathway, were not present in *Aj*TLR3 (70). In addition, we found that the protein sequence of *Aj*TLR3 was close to that of

ASBMB

human *Aj*TLR2 (42), which indicated that *Aj*TLR3 might function similarly to human TLR2 and could recognize $LPS^{V.\ splendidus}$.

In most mammalian cells, autophagy induced by different PAMPs also requires the E3 ligase TRAF6 (25). Based on TLR stimulation, TRAF6 promotes the K63-linked ubiquitination of Beclin1 to induce TLR-mediated autophagy (26). Inomata *et al.* (31) showed that poly(I:C) stimulation induces autophagy *via* TRIF and TRAF6. In atrophying skeletal muscle, the inhibition of TRAF6 also blocks the expression of K63-linked mono/polyubiquitination and impacts autophagosome formation (71). In our study, we discovered that the protein level of *Aj*TRAF6 and the extent of K63-linked ubiquitination of *Aj*TRAF6 were both significantly increased after challenge with the two types of LPS, although higher levels were found in the $LPS^{E.\ coli}$ group than in the $LPS^{V.\ splendidus}$ group, and the K63-linked ubiquitination of *Aj*TRAF6 was abrogated after *Aj*TLR3, *Aj*Toll, or *Aj*TRAF6 knockdown in these two groups (Fig. 6). Zhan *et al.* (26) reported that TLR3 and TLR4 activation induces autophagy in lung cancer cells through the promotion of TRAF6 ubiquitination, which is similar to our results. Moreover, Shi *et al.* (47) showed that an increased abundance of TRAF6 could promote the K63-linked ubiquitination of Beclin1 in RAW264.7 cells. In our results, we found that the K63-linked ubiquitination of *Aj*Beclin1 was both significantly increased in the $LPS^{E.\ coli}$ and $LPS^{V.\ splendidus}$ groups, and their levels were impaired after *AjTLR3* or *AjToll* knockdown (Fig. 7), we speculated that *Aj*TLR3 or *Aj*Toll induces the K63-linked ubiquitination of *Aj*TRAF6, which is essential for the activation of *Aj*Beclin1 ubiquitination. To determine whether *Aj*TRAF6 interacts with *Aj*Beclin1 in coelomocyte, an immunoprecipitation assay was performed. We found that *Aj*Beclin1 can directly combine with *Aj*TRAF6; moreover, our results clearly indicated that the *Aj*TRAF6-deficient coelomocyte exhibited impaired *Aj*Beclin1 ubiquitination (Fig. 7), which suggested that the involvement of *Aj*TRAF6 in the ubiquitination of *Aj*Beclin1 is important for both types of LPS-induced autophagy. In mouse and human species, the ubiquitination of Lys^{117} of Beclin1 could promote the oligomerization of Beclin1 and affect the activity of PI3KC3, which further results in formation of the PI3KC3-Beclin1 protein complex and the induction of autophagy (25, 51). In our study, we identified seven central proteins related to the PI3KC3 complex, such as *Aj*PI3KC3, *Aj*AMBRA1, and related regulatory subunits, which indicates that the nucleation of autophagosomes is highly conserved in *A. japonicus* compared with vertebrates.

A question that remains unaddressed is how challenge with different LPS types causes discrepant autophagy levels. A20 is a known ubiquitin-editing enzyme that mainly functions as an endogenous regulator of inflammation through the termination of NF-κB activation (34) and plays negative roles in the activation of autophagy by limiting TRAF6 E3 ligase activity and directly deubiquitinating Beclin1 (25). First, we found that the protein level of *Aj*A20 was only markedly induced after $LPS^{V.\ splendidus}$ stimulation but not in $LPS^{E.\ coli}$ group under the same conditions (Fig. 7). Because A20 reduces the ubiquitination of Beclin1 and limits the induction of autophagy (25), we hypothesized that the reduction in the autophagy level observed in the $LPS^{V.\ splendidus}$ group might be mediated by *Aj*A20. To more directly test the mechanism responsible for the discrepant autophagy levels induced by $LPS^{V.\ splendidus}$ and $LPS^{E.\ coli}$ challenge, we analyzed the *Aj*Beclin1 ubiquitination and *Aj*A20 expression levels in response to stimulation with two different LPSs after reducing the progression of TLR cascades using specific siRNA. We found that the increase in the *Aj*A20 protein level was abolished by the silencing of *AjTLR3* under the same conditions, which suggested that *Aj*TLR3 signaling under $LPS^{V.\ splendidus}$ stimulation induced the expression of the gene encoding *Aj*A20. Moreover, the *Aj*A20 protein level after $LPS^{V.\ splendidus}$ stimulation was significantly increased by the silencing of *AjTRAF6*, and this finding indicated that this strong expression of *Aj*A20 might lead to a reduction in the extent of ubiquitination of *Aj*Beclin1, which acts to limit autophagy under $LPS^{V.\ splendidus}$ challenge. Most studies have reported that A20 overexpression can inhibit autophagy by limiting the K63-linked ubiquitination of TRAF6 or by directly deubiquitinating Beclin1 (47, 72). Thus, the precise mechanism of *Aj*A20 and deubiquitination should be verified in future studies.

In conclusion, this study shows that *V. splendidus* induces autophagy through the activation of *Aj*TLR3 signaling, but *E. coli* promotes autophagy *via* activation of the *Aj*Toll pathway (Fig. 8). Through these signaling pathways, ubiquitinated *Aj*TRAF6 directly ubiquitinates *Aj*Beclin1, which results in its ubiquitination and subsequently the induction of autophagy. The difference indicates that *Aj*A20 plays a negative regulatory role in the activation of autophagy after $LPS^{V.\ splendidus}$ stimulation. Overall, our study reveals that LPS utilizes diverse mechanisms to induce xenophagy in invertebrate marine animals.

Experimental procedures

Ethics statement

The sea cucumbers used in this work were commercially cultured animals, and all experiments were conducted in accordance with the recommendations in the Guide for the Care and Use of Laboratory Animals of the National Institutes of Health. The study protocol was approved by the Experimental Animal Ethics Committee of Ningbo University, China.

Homology analysis of autophagy machinery

The *A. japonicus* autophagy-related genes that regulate the autophagy machinery were screened from the sea cucumber genome (https://www.ncbi.nlm.nih.gov/assembly/GCA_002754855.1) and transcriptome database (accession number of SRA080354). We used the Protein BLAST program of NCBI (https://www.ncbi.nlm.nih.gov/) to search for other Atg homologs using the *A. japonicus* Atg protein sequences collected from the UniProt database. The conserved domains, signal peptides, and internal repeats of all the proteins were detected using the Simple Modular Architecture Research Tool (SMART) program.

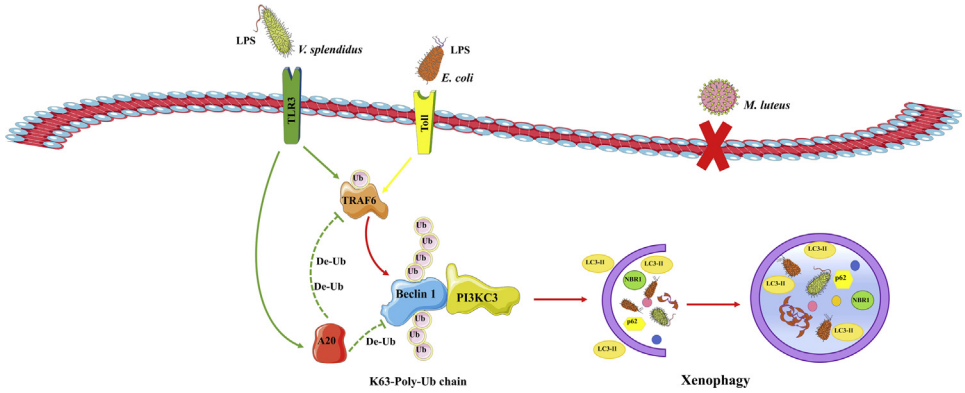

Figure 8. Differential TLR-mediated xenophagy in *A. japonicus* after *V. splendidus* and *E. coli* infection. The exposure of coelomocyte to $LPS^{V.\ splendidus}$ and $LPS^{E.\ coli}$ were mediated by *Aj*TLR3 and *Aj*Toll, respectively. Activated *Aj*TLR3 and *Aj*Toll both promoted *Aj*TRAF6 ubiquitination, which further increased the K63-linked ubiquitination of *Aj*Beclin1 and triggered the formation of autophagosomes. Inconsistently, the engagement of *Aj*TLR3 also triggered a signaling pathway that led to the expression of *Aj*A20. The increased abundance of *Aj*A20 might limit *Aj*TLR3-induced autophagy through the deubiquitination of *Aj*Beclin1. The precise mechanism of A20 and deubiquitination should be verified in future studies. The *yellow solid line* indicates *E. coli*-induced autophagy based on the *Aj*Toll signaling pathway; the *green solid* and imaginary lines indicate *V. splendidus*-induced autophagy based on the *Aj*TLR3 signaling pathway; the *red solid line* indicates the common xenophagy processes in both *V. splendidus*- and *E. coli*-induced autophagy.

Animals and challenge experiments

Three-hundred healthy adult sea cucumbers (116 ± 14 g) were collected from the Dalian Pacific Aquaculture Company and acclimatized in seawater (salinity, 28; temperature, 16 °C) for 3 days. The *A. japonicus* pathogenic microorganism *V. splendidus* was initially isolated from skin ulcer syndrome (SUS)-diseased sea cucumbers. Two other nonpathogenic microorganisms, *E. coli* and *M. luteus*, were maintained in our laboratory. The three bacteria were inoculated in liquid 2216E, LB, and nutrient broth media at 28, 37, and 35 °C, respectively, and shaken at 220 rpm overnight. The culture medium was centrifuged at 5000*g* for 5 min to harvest the bacteria, and the cells were then resuspended in filtered seawater. The sea cucumbers were equally divided into three tanks, and each tank contained 24 sea cucumbers. Each group of *A. japonicus* was infected with the corresponding bacterial species by immersion at a final concentration of 1×10^7 CFU ml^{-1}. For Chloroquine (CQ, dissolved in RNase-free H_2O) and Bafilomycin A1 (Baf-A1) treatments, half of sea cucumbers were injected with 60 μM CQ or 10 nM Baf-A1 *via* their tentacles. Coelomic fluids were collected at 0, 12, and 24 h post infection by dissecting the cavities of the sea cucumbers using sterilized scissors, and the coelomic fluids were filtered through 200-mesh filters. Three sea cucumbers were collected at 0 h in each group served as a control. The collected fluids were centrifuged at 800*g* and 4 °C for 5 min to harvest the coelomocyte. The collected coelomocyte was used for the detection of the corresponding protein levels and immunofluorescence analysis. In addition, three collected bacteria were washed twice in filtered seawater and injected into sea cucumber through tentacles at an MOI of 10 (bacteria: coelomocyte = 10:1) and combined with 10 nM Baf-A1. After 24 h, the coelomocyte was collected and washed with PBS. Then, gentamicin was added to a final concentration of 10 mg ml^{-1} to kill the extracellular bacteria. The collected samples were used for detection of autophagosomes. The percentage of intracellular bacteria in autophagosomes was determined within in 1000 coelomocytes in each group.

Cell culture, LPS, or PGN isolation and exposure

Primary coelomocytes were prepared according to our previous work (73). Briefly, the harvested cells at a final concentration of 10^6 cells ml^{-1} were resuspended in L-15 cell culture medium (Invitrogen) containing penicillin (100 U ml^{-1}) and streptomycin sulfate (100 mg ml^{-1}). NaCl solution was utilized to adjust the osmotic pressure to a final concentration of 0.39 M. The cells were then dispensed into a 24-well culture microplate with 500 μl of L-15 medium in each well, and the cell viability was checked by trypan blue (Solarbio). For LPS stimulation experiments, LPS was isolated from the two bacteria (*E. coli* and *V. splendidus*) using an LPS extraction kit (Beibokit) following the manufacturer's instructions. PGN was isolated from *M. luteus* (Sigma). The cultured cells were exposed to 10 μg ml^{-1} LPS from *E. coli* ($LPS^{E.\ coli}$), 10 μg ml^{-1} LPS from *V. splendidus* ($LPS^{V.\ splendidus}$), or 10 μg ml^{-1} PGN from *M. luteus* ($PGN^{M.\ luteus}$) for 0, 6, and 12 h. Primary cells was collected at 0 h in each group served as a control. For CQ and Baf-A1 treatments, primary coelomocytes were treated with 10 μM CQ or 2 nM Baf-A1. After challenge, the cells were collected and used for subsequent detection of autophagosome formation, determination of the protein levels of autophagy-related genes, and immunofluorescence assays.

RNA interference

Specific siRNAs for *AjTLR3*, *AjToll*, *AjNLRC4*, *AjSR-B*, *AjTRAF6*, and *AjULK* (36) were synthesized by GenePharma (Table S2). Control siRNA (Negative control, NC) that did not target any of the genes from the sea cucumber transcriptome served as a control. The experimental and control siRNAs were dissolved in RNase-free H_2O to obtain 20 μM stock solutions. Approximately 1 μl of each stock solution of siRNA

(final concentration of 80 nM) or 2 μl of the NC was mixed with 1 μl of the siRNA-Mate transfection reagent. The mixture was added to primary cultured cells at 10^6 cells ml^{-1} in each well for 24 h. After interference for 24 h, the coelomocytes were exposed to the two types of LPS (10 μg ml^{-1}) for 0 (control), 6, and 12 h. The harvested primary coelomocytes were used for qPCR, immunoprecipitation, Western blotting, and immunofluorescence assays.

RNA isolation and real-time quantitative PCR

Total RNA was isolated using RNAiso Plus (TaKaRa), and cDNA was synthesized using a PrimeScript RT Reagent Kit with gDNA Eraser (TaKaRa). The relative mRNA expression of each gene was measured using an Applied Biosystem 7500 Real-time Quantitative PCR System (Thermo Fisher Scientific). The specific primers are listed in Table S2. *Aj*β-actin was determined to be a suitable housekeeping gene for the normalization of target quantification by Zhao *et al.* (74). Each reaction was performed in a final volume of 20 μl, which contained 2 μl of cDNA, 1 μl of each primer (10 μM), 6 μl of RNase-free H_2O, and 10 μl of SYBR Green PCR Master Mix (TaKaRa). The amplification procedure was as follows: denaturation at 94 °C for 2 min followed by 40 cycles of 94 °C for 15 s, 60 °C for 20 s, and 72 °C for 30 s. After the cycling stage, melting curve analyses were performed. The $2^{-\Delta\Delta CT}$ method was used to analyze the expression level of each gene (75).

Transmission electron microscopy (TEM)

After the sea cucumbers were challenged with three types of bacteria *in vivo* and subjected to different LPS stimulations *in vitro*, the coelomocytes were harvested as previously described, respectively. First, the collected coelomocytes were washed twice with sterilized isotonic buffer (0.001 M EGTA, 0.53 M NaCl, and 0.01 M Tris-HCl, pH 7.6). The pellets were then fixed in 2.5% glutaraldehyde in PBS at 4 °C for 2 h and washed once with 0.1 M PBS. Subsequently, the pellets were fixed in 1% osmium tetroxide for 1.5 h, dehydrated through a series of ethanol concentrations, and embedded in Epon resin. The samples were sectioned with a microtome, and the sections were double stained with 3% uranyl acetate and lead citrate before examination under a transmission electron microscope.

Antibody preparation

Several recombinant proteins were prepared and used to generate mouse polyclonal antibodies (*e.g.*, *Aj*p62, *Aj*Beclin1, and *Aj*A20) or rabbit polyclonal antibodies (*e.g.*, *Aj*LAMP) according to our previous work (76). Briefly, the partial cDNA sequences of the above genes were cloned with specific primers (Table S2), double digested with restriction enzymes, and ligated into the pET28a(+) vector. The recombinant plasmids were then transformed into *E. coli* Rosetta (DE3) cells (Invitrogen), generated by adding IPTG at a final concentration of 1 mM, and purified using a nickel-nitrilotriacetic acid (Ni-NTA) column (QIAGEN). After dialysis, the soluble target proteins were injected into 4-week-old mice or rabbits to acquire polyclonal antibodies according to our previously described protocol (76). In addition, antibodies against Ub-K63 (T56579S), β-actin (M20011S), TRAF6 (T55175S), Beclin1 (T55092S) were purchased from Abmart. HRP-conjugated anti-mouse (D110087) and anti-rabbit IgG (D110058) secondary antibodies were purchased from Sangon. Antibody against LC3B (ab51520) was purchased from ABCAM.

Immunofluorescence analysis

The tested coelomocytes obtained as above were seeded at a density of approximately 10^5 cells ml^{-1} on glass chamber slides with lysine and treated for 20 min at 16 °C. Thereafter, the supernatant from two independent experiments was discarded, and the coelomocytes in each well were fixed with 4% paraformaldehyde (PFA) for 30 min and permeabilized with 0.1% Triton X-100 (Sigma) for 10 min. The cells were washed three times with PBST (PBS containing 0.05% Tween-20) and blocked with 5% BSA in PBS at 25 °C for 1 h. The supernatant was then removed, and the cells were incubated overnight with anti-LC3B antibody (1:500 dilution) or the combination of anti-LC3B antibody and anti-LAMP antibody (1:500 dilution) as the primary antibodies at 4 °C. After three washes with PBST, the cells incubated with the anti-LC3B antibody alone were incubated with an FITC-conjugated goat anti-mouse secondary antibody (1:1000 dilution) at 37 °C for 1 h, and the cells incubated with two primary antibodies were further incubated with Cy3-conjugated goat anti-rabbit (1:1000 dilution) and FITC-conjugated goat anti-mouse secondary antibodies for 1 h at 37 °C. After three additional washes with PBST, DAPI (diluted to 10 μg ml^{-1} in PBS; Beyotime Biotechnology) was added to the cells to stain the nuclei. After a final three cycles of washing, the cells were mounted in antifade fluorescence mounting medium for observation with a laser-scanning confocal microscope (ZEISS).

Western blotting analysis

Western blotting analysis was performed as described in our previous work (73). The proteins from coelomocytes were extracted using cell lysis buffer (Beyotime Biotechnology), and the concentration was measured with a BCA protein assay kit (Sangon). Approximately 50 μg of protein in each well was separated by SDS-PAGE with a gel thickness of 1 mm and then electrophoretically transferred to a 0.45-μm-pore-size nitrocellulose membrane. The membrane was blocked with 5% skim milk at 25 °C for 1 h and then incubated with specific polyclonal antibodies (usually diluted 1:1000 in 5% skim milk) at 4 °C overnight. Subsequently, the membranes were washed three times with TBST (20 mM Tris-HCl, 150 mM NaCl, 0.05% Tween-20) and incubated with the corresponding secondary antibodies (usually diluted 1:3000 in 5% skim milk) at 25 °C for 1.5 h. The membranes were then subjected to three 10 min washes with TBST, incubated with Western Lightning-ECL substrate (PerkinElmer) and exposed to X-OMAT AR X-ray film (Eastman Kodak). The protein and *Aj*β-actin bands were quantified using the BioRad Quantity One software

package, and the results were derived from a statistical analysis of three independent experiments.

Immunoprecipitation and ubiquitination

For coimmunoprecipitation assays, LPS-exposed coelomocytes were lysed in a buffer that contained 20 mM HEPES pH 7.4, 50 mM β-glycerophosphate, 1 mM Na_3VO_4, 0.5% Triton X-100, 0.5% CHAPS, and 10% glycerol with a protease inhibitor cocktail (Beyotime Biotechnology). The equal lysates were incubated with equal anti-*Aj*TRAF6 or anti-*Aj*Beclin1 antibody overnight at 4 °C and then incubated with Protein A + G Agarose (Beyotime Biotechnology) for 4 h at 4 °C. The immunoprecipitates were collected, washed four times with lysis buffer, and analyzed by SDS-PAGE and immunoblotting. For the detection of *Aj*TRAF6 or *Aj*Beclin1 ubiquitination, the samples were first incubated with an antibody against K63-linked ubiquitination overnight at 4 °C. The membrane was subjected to three 10 min washes with TBST and then incubated with HRP-conjugated secondary antibody at 25 °C for 1.5 h. After three 10 min washes with TBST, the membrane was incubated with Western Lightning-ECL substrate and exposed to X-OMAT AR X-ray film. To determine whether *Aj*Beclin1 directly interacts with *Aj*TRAF6, the membrane was stripped and then incubated with an antibody against *Aj*Beclin1. The subsequent steps were the same as those described above. Because the protein molecular weight of *Aj*Beclin1 was similar with heavy chain of the antibody, we used Goat Anti-Rabbit IgG HRP (M21008S, Abmart), which could remove both heavy chain of the antibody and light chain of the antibody.

Statistical analysis

Both *in vivo* and *in vitro* experiments were executed with three biological replicates, and the data are expressed as the means ± standard deviations (SDs) (n = 3). One-way ANOVA was applied to determine the significance of the differences between the control and experimental groups. Differences were considered significant at $^{*}p < 0.05$ and $^{**}p < 0.01$.

Data availability

Requests for access to the data, statistical code, questionnaires, and technical processes may be made by contacting the corresponding author at lichenghua@nbu.edu.cn.

Supporting information—This article contains supporting information

Acknowledgments—This work was supported by the National Natural Science Foundation of China (32073003), Natural Science Foundation of Zhejiang Province (LZ19C190001), K. C. Wong Magna Fund in Ningbo University and the Bio-ultrastructure Analysis Laboratory of the Key Laboratory of Applied Marine Biotechnology of the Ministry of Education, Ningbo University.

Author contributions—C. L., Y. S., and Z. W. conceptualization; Y. S., Z. W., C. Z., and D. L. formal analysis; Z. W., K. C., Y. S., and Z. L. investigation; C. L., Y. S., and Z. W. methodology; C. L. and W. Z. resources; Y. S., C. L., and Z. W. writing—original draft.

Conflict of interest—We declare that we have no conflict of interest. The *A. japonicus* were commercially cultured animals, and all the experiments were conducted in accordance with the recommendations in the Guide for the Care and Use of Laboratory Animals of the National Institutes of Health. The study protocol was approved by the Experimental Animal Ethics Committee of Ningbo University, China.

Abbreviations—The abbreviations used are: Baf-A1, Bafilomycin A1; CLIR, noncanonical LIR; CQ, Chloroquine; dsRNA, double-stranded RNALPSs; GABARAP, gamma-aminobutyric acid receptor-associated protein; GATE16, Golgi-associated ATPase enhancer of 16 kDa; LC3, microtubule-associated protein 1 light chain 3; LIR, LC3-interacting region; LPSs, lipopolysaccharides; MARCO, macrophage receptor with collagenous structure; MSCs, human mesenchymal stem cells; Ni-NTA, nickel-nitrilotriacetic acid; NLRs, NOD-like receptors; NOD1, nucleotide-binding oligomerization domain 1; OTU, ovarian tumor; PAMP, pathogen associated molecular pattern; PFA, paraformaldehyde; PGN, peptidoglycan; PGRP, peptidoglycan-recognition protein; PI3KC3, class III phosphatidylinositol 3-kinase complex; poly(I:C), polyinosinic-polycytidylic acid; PRRs, pattern recognition receptors; SD, standard deviation; SMART, Simple Modular Architecture Research Tool; SR-B1, scavenger receptor-B1; ssRNA, single-stranded RNA; SUS, skin ulcer syndrome; TLRs, Toll/Toll-like receptors; UBDs, ubiquitin-binding domains; UBR, ubiquitin-binding region.

References

1. de Duve, C. (2007) The origin of eukaryotes: A reappraisal. *Nat. Rev. Genet.* **8**, 395–403
2. Scott, R. C., Schuldiner, O., and Neufeld, T. P. (2004) Role and regulation of starvation-induced autophagy in the *drosophila* fat body. *Dev. Cell* **7**, 167–178
3. He, C., and Klionsky, D. (2009) Regulation mechanisms and signaling pathways of autophagy. *Annu. Rev. Genet.* **43**, 67–93
4. Puri, C., Vicinanza, M., and Rubinsztein, D. C. (2018) Phagophores evolve from recycling endosomes. *Autophagy* **14**, 1475–1477
5. Yu, L., Chen, Y., and Tooze, S. A. (2018) Autophagy pathway: Cellular and molecular mechanisms. *Autophagy* **14**, 207–215
6. Reggiori, F., and Ungermann, C. (2017) Autophagosome maturation and fusion. *J. Mol. Biol.* **429**, 486–496
7. Mizushima, N. (2020) The ATG conjugation systems in autophagy. *Curr. Opin. Cell Biol.* **63**, 1–10
8. Kabeya, Y., Mizushima, N., Ueno, T., Yamamoto, A., Kirisako, T., Noda, T., Kominami, E., Ohsumi, Y., and Yoshimori, T. (2000) LC3, a mammalian homologue of yeast Apg8p, is localized in autophagosome membranes after processing. *EMBO J.* **19**, 5720–5728
9. Zaffagnini, G., and Martens, S. (2016) Mechanisms of selective autophagy. *J. Mol. Biol.* **428**, 1714–1724
10. Stolz, A., Ernst, A., and Dikic, I. (2014) Cargo recognition and trafficking in selective autophagy. *Nat. Cell Biol.* **16**, 495–501
11. Cong, Y., Kumar, N. D., Mauthe, M., Verlhac, P., and Reggiori, F. (2020) Manipulation of selective macroautophagy by pathogens at a glance. *J. Cell Sci.* **133**, jcs240440
12. Thurston, T. L., Ryzhakov, G., Bloor, S., Muhlinen, N., and Randow, F. (2009) The TBK1 adaptor and autophagy receptor NDP52 restricts the proliferation of ubiquitin-coated bacteria. *Nat. Immunol.* **10**, 1215–1221

13. Mostowy, S., Sancho-Shimizu, V., Hamon, M. A., Simeone, R., Brosch, R., Johansen, T., and Cossart, P. (2011) p62 and NDP52 proteins target intracytosolic shigella and listeria to different autophagy pathways. *J. Biol. Chem.* **286**, 26987–26995
14. Dupont, N., Lacas-Gervais, S., Bertout, J., Paz, I., Freche, B., Nhieu, G. T. V., Gisou van der Goot, F., Sansonetti, P. J., and Lafont, F. (2009) *Shigella* phagocytic vacuolar membrane remnants participate in the cellular response to pathogen invasion and are regulated by autophagy. *Cell Host Microbe* **6**, 137–149
15. Greenfield, L. K., and Jones, N. L. (2013) Modulation of autophagy by *Helicobacter pylori* and its role in gastric carcinogenesis. *Trends Microbiol.* **21**, 602–612
16. Tang, D., Kang, R., Coyne, C. B., Zeh, H. J., and Lotze, M. T. (2012) PAMPs and DAMPs: Signals that spur autophagy and immunity. *Immunol. Rev.* **49**, 158–175
17. Sharma, V., Verma, S., Seranova, E., Sarkar, S., and Kumar, D. (2018) Selective autophagy and xenophagy in infection and disease. *Front. Cell Dev. Biol.* **6**, 1–17
18. Delgado, M. A., and Deretic, V. (2009) Toll-like receptors in control of immunological autophagy. *Cell Death Differ.* **16**, 976–983
19. Khan, A., Mann, L., Papanna, R., Lyu, M. A., Singh, C. R., Olson, S., Eissa, N. T., Cirillo, J., Das, G., and Hunter, R. L. (2017) Mesenchymal stem cells internalize *Mycobacterium tuberculosis* through scavenger receptors and restrict bacterial growth through autophagy. *Sci. Rep.* **7**, 15010
20. Travassos, L. H., Carneiro, L. A., Ramjeet, M., Hussey, S., Kim, Y. G., Magalhes, J. G., Yuan, L., Soares, F., Chea, E., Bourhis, L. L., Boneca, I. G., Allaoui, A., Jones, N. L., Nuñez, G., Girardin, S. E., *et al.* (2010) Nod1 and Nod2 direct autophagy by recruiting ATG16L1 to the plasma membrane at the site of bacterial entry. *Nat. Immunol.* **11**, 55–62
21. Heil, F., Hemmi, H., Hochrein, H., Ampenberger, F., Kirschning, C., Akira, S., Lipford, C., Wagner, H., and Bauer, S. (2004) Species-specific recognition of single-stranded RNA via toll-like receptor 7 and 8. *Science* **303**, 1526–1529
22. Gorden, K. K., Qiu, X. X., Binsfeld, C. C. A., Vasilakos, J. P., and Alkan, S. S. (2006) Cutting edge: Activation of murine TLR8 by a combination of imidazoquinoline immune response modifiers and polyT oligo-deoxynucleotides. *J. Immunol.* **177**, 6584–6658
23. Yano, T., Mita, S., Ohmori, H., Oshima, Y., Fujimoto, Y., Ueda, R., Takada, H., Goldman, W. E., Fukase, K., Silverman, N., Yoshimori, T., and Kurata, S. (2008) Autophagic control of listeria through intracellular innate immune recognition in drosophila. *Nat. Immunol.* **9**, 908–916
24. Kurata, S. (2010) Extracellular and intracellular pathogen recognition by *Drosophila* PGRP-LE and PGRP-LC. *Int. Immunol.* **22**, 143–148
25. Shi, C. S., and Kehrl, J. H. (2010) TRAF6 and A20 regulate lysine 63-linked ubiquitination of Beclin-1 to control TLR4-induced autophagy. *Autophagy* **3**, 1–10
26. Zhan, Z. Z., Xie, X. F., Cao, H., Zhou, X., and Xu, D. Z. (2014) Autophagy facilitates TLR4- and TLR3-triggered migration and invasion of lung cancer cells through the promotion of TRAF6 ubiquitination. *Autophagy* **10**, 257–268
27. Grumati, P., and Dikic, I. (2018) Ubiquitin signaling and autophagy. *J. Biol. Chem.* **293**, 5404–5413
28. Fusco, C., Mandriani, B., Rienzo, M. D., Micale, L., Malerba, N., Cocciadiferro, D., Sjøttem, E., Augello, B., Squeo, G., Pellico, M. T., Jain, A., Johansen, T., Fimia, G. M., and Merla, G. (2018) TRIM50 regulates Beclin 1 proautophagic activity. *Biochim. Biophys. Acta Mol. Cell Res.* **1865**, 908–919
29. Xu, C. F., Feng, K., Zhao, X. N., Huang, S. Q., Cheng, Y. J., Qian, L., Wang, Y. N., Sun, H. X., Jin, M., Chuang, T., and Zhang, Y. Y. (2014) Regulation of autophagy by E3 ubiquitin ligase RNF216 through BECN1 ubiquitination. *Autophagy* **10**, 2239–2250
30. Abada, A., and Elazar, Z. (2014) Getting ready for building: Signaling and autophagosome biogenesis. *EMBO Rep.* **15**, 839–852
31. Inomata, M., Niida, S., Shibata, K., and Into, T. (2012) Regulation of Toll-like receptor signaling by NDP52-mediated selective autophagy is normally inactivated by A20. *Cell. Mol. Life Sci.* **69**, 963–979
32. Martens, A., and van Loo, G. (2020) A20 at the crossroads of cell death, inflammation, and autoimmunity. *Cold Spring Harb. Perspect. Biol.* **12**, a036418
33. Shu, D. G., Morris, S. C., Han, J., Zhang, Z. F., and Liu, J. N. (2004) Ancestral echinoderms from the Chengjiang deposits of China. *Nature* **430**, 422–428
34. Han, Q., Keesing, J. K., and Liu, D. (2016) A review of sea cucumber aquaculture, ranching, and stock enhancement in China. *Rev. Fish. Sci. Aquac.* **24**, 326–341
35. Parzych, K. R., and Klionsky, D. J. (2014) An overview of autophagy: Morphology, mechanism, and regulation. *Antioxid. Redox Signal.* **20**, 460–473
36. Chen, K. Y., Shao, Y. N., and Li, C. H. (2021) ULK induces autophagy by targeting Beclin-1 in *Vibrio splendidus* challenged *Apostichopus japonicus*. *Aquaculture* **532**, 736022
37. Zhang, P. J., Li, C. H., Zhu, L., Su, X. R., Li, Y., Jin, C. H., and Li, T. W. (2013) *De novo* assembly of the sea cucumber *Apostichopus japonicus* hemocytes transcriptome to identify miRNA targets associated with skin ulceration syndrome. *PLoS One* **8**, e73506
38. Li, Y. L., Wang, R. J., Xun, X. G., Wang, J., Bao, L. S., Thimmappa, R., Ding, J., Jiang, J. W., Zhang, L. H., Li, T. Q., Lv, J., Mu, C., Hu, X. L., Zhang, L. L., Liu, J., *et al.* (2018) Sea cucumber genome provides insights into saponin biosynthesis and aestivation regulation. *Cell Discov.* **4**, 1–17
39. Zhang, X., Sun, L. N., Yuan, J., Sun, Y., Gao, Y., Zhang, L., Li, S., Dai, H., Hamel, J. F., Liu, C., Yu, Y., Liu, S., Lin, W., Guo, K., Jin, S., *et al.* (2017) The sea cucumber genome provides insights into morphological evolution and visceral regeneration. *PLoS Biol.* **15**, e2003790
40. Verheye, S., Martinet, W., Kockx, M. M., Knaapen, M. W. M., Salu, K., Timmermans, J., Ellis, J. T., Kilpatrick, D. L., and De Meyer, G. R. Y. (2007) Selective clearance of macrophages in atherosclerotic plaques by autophagy. *J. Am. Coll. Cardiol.* **49**, 706–715
41. Chen, M., Liu, J. X., Yang, W. Q., and Ling, W. H. (2017) Lipopolysaccharide mediates hepatic stellate cell activation by regulating autophagy and retinoic acid signaling. *Autophagy* **13**, 1813–1827
42. Sun, H. J., Zhou, Z. C., Dong, Y., Yang, A. F., Jiang, B., Gao, S., Chen, Z., Guan, X. Y., Wang, B., and Wang, X. L. (2013) Identification and expression analysis of two Toll-like receptor genes from sea cucumber (*Apostichopus japonicus*). *Fish Shellfish Immunol.* **34**, 147–158
43. Chen, K. Y., Lv, Z. M., Shao, Y. N., Guo, M., and Li, C. H. (2020) Cloning and functional analysis the first NLRC4-like gene from the sea cucumber *Apostichopus japonicus*. *Dev. Comp. Immunol.* **104**, 103541
44. Che, Z. J., Shao, Y. N., Zhang, W. W., Zhao, X. L., and Li, C. H. (2019) Cloning and functional analysis of scavenger receptor B gene from the sea cucumber *Apostichopus japonicus*. *Dev. Comp. Immunol.* **99**, 103404
45. Verstak, B., Stack, J., Ve, T., Mangan, M., Hjerrild, K., Jeon, J., Stahl, R., Latz, E., Gay, N., Kobe, B., Bowie, A. G., and Mansell, A. (2014) The TLR signaling adaptor TRAM interacts with TRAF6 to mediate activation of the inflammatory response by TLR4. *J. Leukoc. Biol.* **96**, 427–436
46. Chan, S. T., Lee, J., Narula, M., and Ou, J. J. (2016) Suppression of host innate immune response by Hepatitis C virus via induction of autophagic degradation of TRAF6. *J. Virol.* **90**, 10928–10935
47. Shi, C. S., and Kehrl, J. H. (2010) Traf6 and A20 differentially regulate TLR4-induced autophagy by affecting the ubiquitination of Beclin 1. *Autophagy* **6**, 986–987
48. Dinkins, C., Pilli, M., and Kehrl, J. H. (2015) Roles of autophagy in HIV infection. Immunol. *Cell Biol.* **93**, 11–17
49. Li, X., Chen, D., Hua, Q. Q., Wan, Y. J., Zheng, L. N., Liu, Y. Y., Lin, J. X., Pan, C. W., Hu, X., and Tan, F. (2016) Induction of autophagy interferes the tachyzoite to bradyzoite transformation of *Toxoplasma gondii*. *Parasitology* **143**, 639–645
50. Maruyama, T., and Noda, N. N. (2017) Autophagy-regulating protease Atg4: Structure, function, regulation and inhibition. *J. Antibiot.* **71**, 72–78
51. Xie, Z. P., and Klionsky, D. J. (2007) Autophagosome formation: Core machinery and adaptations. *Nat. Cell Biol.* **9**, 1102–1109
52. Juretschke, T., Beli, P., and Dikic, I. (2019) Quantitative phosphoproteomics of selective autophagy receptors. *Methods Mol. Biol.* **1880**, 691–701
53. Deretic, V., Saitoh, T., and Akira, S. (2013) Autophagy in infection, inflammation and immunity. *Nat. Rev. Immunol.* **13**, 722–737

54. Gibson, J. F., Gibson, T. K., Hill, C. J., Tooke, A. K., Serba, J. J., Tonge, R. D., Foster, S. J., Grierson, A. J., Ingham, P. W., Renshaw, S. A., and Johnston, S. A. (2021) Neutrophils use selective autophagy receptor Sqstm1/p62 to target *Staphylococcus aureus* for degradation *in vivo* in zebrafish. *Autophagy* **17**, 1–10
55. Hu, Z. G., Cao, X. B., Guo, M., and Li, C. H. (2020) Identification and characterization of a novel short-type peptidoglycan recognition protein in *Apostichopus japonicus*. *Fish Shellfish Immunol.* **299**, 257–266
56. Zhang, Y., Yao, Y., Qiu, X., Wang, G. D., Hu, Z., Chen, S. Y., Wu, Z. X., Yuan, N., Gao, H. C., Wang, J. R., Song, H. H., Girardin, S. E., and Qian, Y. C. (2019) Listeria hijacks host mitophagy through a novel mitophagy receptor to evade killing. *Nat. Immunol.* **20**, 433–446
57. Juárez, E., Carranza, C., Hernández-Sánchez, F., León-Contreras, J. C., Hernández-Pando, R., Escobedo, D., Torres, M., and Sada, E. (2012) NOD2 enhances the innate response of alveolar macrophages to *Mycobacterium tuberculosis* in humans. *Eur. J. Immunol.* **42**, 880–889
58. Liu, W., Zhuang, J., Jiang, Y., Chen, J., Sun, J., Jiao, X., and Xu, X. (2019) Toll-like receptor signalling cross-activates the autophagic pathway to restrict *Salmonella* Typhimurium growth in macrophages. *Cell Microbiol.* **21**, e13095
59. Beutler, B., and Rietschel, E. T. (2003) Innate immune sensing and its roots: The story of endotoxin. *Nat. Rev. Immunol.* **3**, 169–176
60. Xu, Y., Jagannath, C., Liu, X. D., Sharafkhaneh, A., Kolodziejska, K. E., and Eissa, N. T. (2007) Toll-like receptor 4 is a sensor for autophagy associated with innate immunity. *Immunity* **27**, 135–144
61. Doyle, A., Zhang, G. H., Fattah, E. A. A., Eissa, N. T., and Li, Y. P. (2011) Toll-like receptor 4 mediates lipopolysaccharide-induced muscle catabolism via coordinate activation of ubiquitin-proteasome and autophagy-lysosome pathways. *FASEB J.* **25**, 99–110
62. Wild, P., Farhan, H., McEwan, D. G., Wagner, S., Rogov, V. V., Brady, N. R., Richter, B., Korac, J., Waidmann, O., Choudhary, C., Dötsch, V., Bumann, D., and Dikic, I. (2011) Phosphorylation of the autophagy receptor optineurin restricts Salmonella growth. *Science* **333**, 228–233
63. Wang, J., Feng, X. R., Zheng, Y. J., Fan, J. J., Wu, J., Li, Z. J., Liu, X. H., Huang, R., Huang, F. X., Yu, X. Q., and amd Yang, X. (2013) Lipopolysaccharide (LPS)-induced autophagy is involved in the restriction of *Escherichia coli* in peritoneal mesothelial cells. *BMC Microbiol.* **13**, 1–16
64. Norris, M. H., Schweizer, H. P., and Tuanyok, A. (2017) Structural diversity of *Burkholderia pseudomallei* lipopolysaccharides affects innate immune signaling. *PLoS Neglect. Trop. Dis.* **11**, e0005571
65. Bortoluci, K. R., and Medzhitov, R. (2010) Control of infection by pyroptosis and autophagy: Role of TLR and NLR. *Cell. Mol. Life Sci.* **67**, 1643–1651
66. Raetz, C. R., and Whitfield, C. (2002) Lipopolysaccharide endotoxins. *Annu. Rev. Biochem.* **71**, 635–700
67. Schromm, A. B., Brandenburg, K., Loppnow, H., Moran, A. P., Koch, M. H. J., Rietschel, E. T. H., and Seydel, U. (2000) Biological activities of lipopolysaccharides are determined by the shape of their lipid A portion. *Eur. J. Biochem.* **267**, 2008–2013
68. Netea, M. G., van Deuren, M., Kullberg, B. J., Cavaillonb, J., and Meer, J. W. M. V. (2002) Does the shape of lipid A determine the interaction of LPS with Toll-like receptors? *Trends Immunol.* **23**, 135–139
69. Nahori, M., Fournié-Amazouz, E., Que-Gewirth, N. S., Balloy, V., Chignard, M., Raetz, C. R. H., Girons, I. S., and Werts, C. (2005) Differential TLR recognition of leptospiral lipid A and lipopolysaccharide in murine and human cells. *J. Immunol.* **175**, 6022–6031
70. Sarkar, S. N., Smith, H. L., Rowe, T. W., and Sen, G. C. (2013) Double-stranded RNA signaling by Toll-like receptor 3 requires specific tyrosine residues in its cytoplasmic domain. *J. Biol. Chem.* **278**, 4393–4396
71. Paul, P. K., and Kumar, A. (2011) TRAF6 coordinates the activation of autophagy and ubiquitin-proteasome systems in atrophying skeletal muscle. *Autophagy* **7**, 555–556
72. Yan, K., Wu, C., Ye, Y., Ye, Y., Li, L., Wang, X. Q., He, W., Ren, S. S., and Xu, Y. (2020) A20 inhibits osteoclastogenesis via TRAF6-dependent autophagy in human periodontal ligament cells under hypoxia. *Cell Prolif.* **53**, e12778
73. Zhang, P. J., Li, C. H., Zhang, R., Zhang, W. W., Jin, C. H., Wang, L. L., and Song, L. S. (2015) The roles of two miRNAs in regulating the immune response of sea cucumber. *Genetics* **201**, 1397–1410
74. Zhao, Y., Chen, M. Y., Wang, T. M., Sun, L. N., Xu, D. W., and Yang, H. S. (2014) Selection of reference genes for qRT-PCR analysis of gene expression in sea cucumber *Apostichopus japonicus* during aestivation. *Chin. J. Oceanol. Limn.* **32**, 1248–1256
75. Livak, K. J., and Schmittgen, T. D. (2001) Analysis of relative gene expression data using real-time quantitative PCR and the $2^{-\Delta\Delta CT}$ method. *Methods* **25**, 5402–5408
76. Wang, Z. H., Lv, Z. M., Li, C. H., Shao, Y. N., and Zhao, X. L. (2018) An invertebrate β-integrin mediates coelomocyte phagocytosis via activation of septin2 and 7 but not septin10. *Int. J. Biol. Macromol.* **113**, 1167–1181